

Geochemistry, Geophysics, Geosystems

RESEARCH ARTICLE

10.1029/2021GC009688

Key Points:

- Out of 165 Holocene volcanoes in the Andes, nine are spatially and geochemically anomalous
- Anomalous arc magmatism can be triggered by melting in response to slab tearing or slab edge effects
- Slab disruptions can be reconstructed by assigning geochemical anomaly scores to volcanic rocks

Supporting Information:

Supporting Information may be found in the online version of this article.

Correspondence to:

G. Rosenbaum,
g.rosenbaum@uq.edu.au

Citation:

Rosenbaum, G., Caulfield, J. T., Ubide, T., Ward, J. F., Sandiford, D., & Sandiford, M. (2021). Spatially and geochemically anomalous arc magmatism: Insights from the Andean arc. *Geochemistry, Geophysics, Geosystems*, 22, e2021GC009688.
<https://doi.org/10.1029/2021GC009688>

Received 29 JAN 2021

Accepted 7 JUN 2021

Spatially and Geochemically Anomalous Arc Magmatism: Insights From the Andean Arc

Gideon Rosenbaum¹ , John T. Caulfield², Teresa Ubide¹ , Jack F. Ward¹ , Dan Sandiford³, and Mike Sandiford⁴

¹School of Earth and Environmental Sciences, The University of Queensland, Brisbane, QLD, Australia, ²Central Analytical Research Facility, Queensland University of Technology, Brisbane, QLD, Australia, ³Institute of Marine and Antarctic Studies, University of Tasmania, Hobart, TAS, Australia, ⁴School of Earth Sciences, University of Melbourne, Melbourne, VIC, Australia

Abstract While most volcanic arcs show a distinctive spatial relationship to subducting plates, there are many examples where volcanoes occur in anomalous locations. These are commonly also geochemically anomalous relative to the composition of more typical subduction-related rocks. Using Holocene volcanoes in South America as a case study, we document the spatial and geochemical patterns along the Andean volcanic belt. To determine whether spatial variations are also geochemically anomalous, we assess a series of geochemical indices that provide information on the depth and degree of melting, and the role of metasomatic subduction inputs in melt generation. We use these parameters to develop a scoring system, with the lowest and highest scores indicating “typical” and “anomalous” arc melting processes, respectively. Typical arc magmatism is defined as melts generated in the sub-arc mantle wedge through slab-derived fluid metasomatism, with or without contributions from subducted sediments. In contrast, we show that anomalous volcanism in South America appears to relate to geometric anomalies in the subducting Nazca plate (e.g., beneath Sumaco, Laguna Blanca and Payun Matru), or to areas affected by variations in mantle flow due to the proximity to the slab edge (Crater Basalt Volcanic Field). By establishing relationships between anomalous magmatism and slab structure, we propose that similar geochemical fingerprints could be used to explore the magmatic response to slab deformation and/or tearing in older arc systems, particularly in cases where the three-dimensional slab structure is no longer detectable.

Plain Language Summary Arc volcanoes, such as those found in the Pacific Ring of Fire, occur in areas where one plate subducts beneath another. Magmas associated with these volcanoes are produced by the release of fluids from the subducting plate. However, some volcanoes in the proximity of subduction zones do not conform to this model, either because they are positioned at unexpected locations relative to the subducting plate and/or because their geochemical compositions cannot be easily reconciled with fluid-induced melting. Focusing on 165 active and dormant volcanoes in the Andes, we document spatial and geochemical patterns that allow us to identify areas of anomalous arc magmatism. We suggest that such anomalies occur in areas where normal subduction processes are disrupted, for example, due to tearing of the subducting plate. Our approach, which involves assigning a geochemical anomaly score to individual analyses, could help identifying similar plate tectonic processes that inevitably occurred in other modern and ancient convergent plate boundaries.

1. Introduction

Arc magmatism in subduction zones is commonly considered as the “factory” for the production of continental crust (Tatsumi, 2005). It is widely agreed that the origin of arc magmatism is controlled by partial melting in the mantle wedge, driven by the release of metasomatic agents from the subducting slab (Grove et al., 2006; Schmidt & Poli, 1998). Therefore, the geometry of the slab is reflected in the spatial distribution of arc volcanoes, which typically occur parallel to the trench and overlying the slab at depths of 124 ± 38 km (Stern, 2002). In addition, arc magmas are typically characterized by geochemical signatures that reflect the local subduction regime, encompassing the angle (depth) of subduction (Syracuse & Abers, 2006), the composition of down-going sediments (Plank & Langmuir, 1998) and slab-derived fluids (Brenan, Shaw, Ryerson, Phinney, 1995b), and slab surface temperatures that influence the nature of metasomatic fluxes

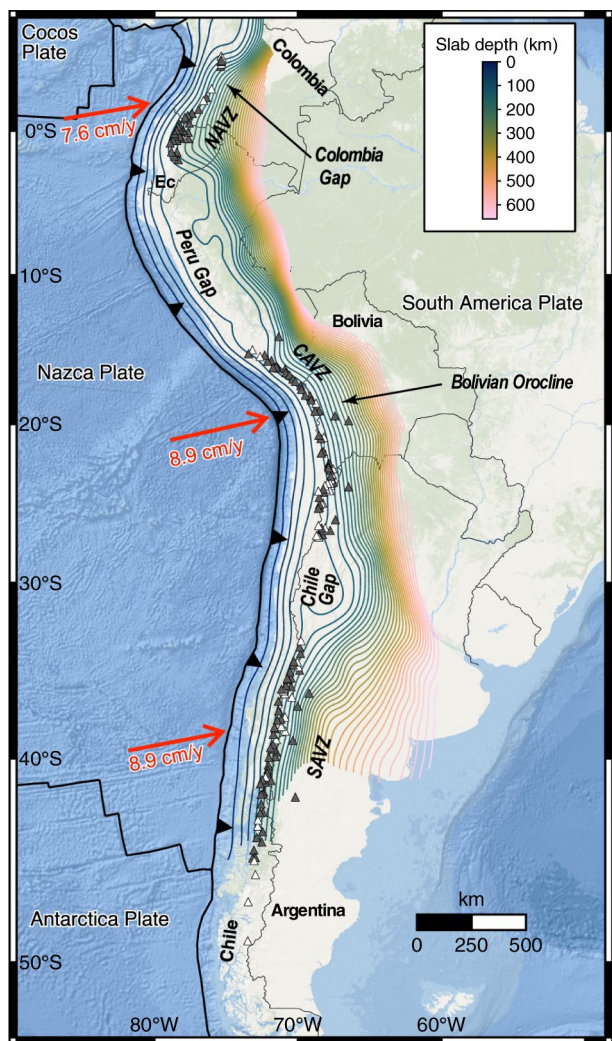


Figure 1. Tectonic map showing Holocene volcanoes in South America (triangles) and slab depth contours (after Hayes et al., 2018). Dark gray and white triangles indicate volcanoes with and without geochemical data, respectively (see Table S1). Red arrows show the present-day convergence vectors at three points along the trench (R. D. Müller et al., 2016). CAVZ, Central Andean Volcanic Zone; Ec, Ecuador; NAVZ, Northern Andean Volcanic Zone; SAVZ, Southern Andean Volcanic Zone.

(Caulfield et al., 2012; Plank et al., 2009). Such processes generally give rise to calc-alkaline magmas that dominate arc settings. Geologists commonly use these spatial and geochemical characteristics to reconstruct the evolution of slabs in recent and ancient magmatic arcs (e.g., Mamani et al., 2010; Rosenbaum & Lister, 2004b; Till et al., 2019), and to search for subduction-related mineral deposits such as porphyry Cu and Au deposits (Wilkinson, 2013). However, there are numerous examples of individual volcanoes and volcanic fields that are spatially and/or geochemically anomalous relative to “typical” arc volcanoes. Commonly, it is these “anomalous” arc magmas that appear to be associated with porphyry ore deposits (D. Müller & Groves, 2019).

In this paper, we coin the term SGAM (Spatially and Geochemically Anomalous Magmatism) to describe subduction-related igneous rocks that do not occur at the expected position relative to the slab, and/or deviate from the representative geochemistry of “typical” arc magmas. An example of SGAM is manifested in Mount Etna (Sicily), which is situated along the edge of the retreating Calabrian slab (Gvirtzman & Nur, 1999) and is spatially anomalous with respect to the volcanic arc. Geochemically, lavas from Mount Etna dominantly belong to the alkaline series, showing geochemical signatures that were likely acquired from an asthenospheric mantle source with limited evidence for a fluid metasomatized origin (Schiano et al., 2001). This anomalous behavior has led many authors to suggest that magmatism in Etna is directly linked to the kinematics and geometry of the retreating Calabrian slab, which allows melt generation by upwelling of asthenospheric material around the slab edge (Doglioni et al., 2001; Gvirtzman & Nur, 1999; Rosenbaum et al., 2008; Schellart, 2010). Elsewhere, SGAM might be represented, for example, by present-day volcanism in the area of the Aleutian-Kamchatka junction (Yogodzinski et al., 2001), and Miocene volcanism in Baja California (Pallares et al., 2007) and western Anatolia (Prelević et al., 2015). Such anomalous magmatism may arise from interactions between mantle dynamics and complex three-dimensional slab structures (Faccenna et al., 2010), but to fully understand these relationships, it is crucial to establish a better definition of SGAM based on systematic spatio-geochemical variations in magmatic arcs.

The aim of this paper is to explore spatial and geochemical connotations that allow a more systematic definition of SGAM, and to discuss possible relationships between SGAM and slab structures. Using Holocene volcanoes in South America (Figure 1), we define the range of spatial and geochemical parameters that constitute a “typical” continental arc environment, and we identify volcanoes that demonstrate substantial deviations

relative to proximal volcanic centers. We then discuss the origin of SGAM in South America in the context of the slab structure. Finally, we discuss the applicability of our results to the recognition of SGAM in older rocks, with the idea that such evidence in the geological record can possibly provide a clue to the origin of subduction perturbations through time and the associated development of mineral deposits.

2. Methods

To understand spatial relationships between Holocene volcanoes in South America and the corresponding slab structure, we use the Slab2 model (Hayes et al., 2018) of the three-dimensional geometry of the subducting slab beneath the Andes. This model incorporates a range of seismic data (e.g., regional and local seismic catalogs, receiver functions, and seismic tomography) to construct a continuous slab (Hayes et al., 2018). As such, it is inevitably beset by inaccuracies and/or inconsistencies (e.g., Sandiford et al., 2020), especially in

Table 1
Parameters Used for the Spatio-Geochemical Analysis

Parameter	Symbol	Comment and reference
Slab depth	Hs	Slab2 (Hayes et al., 2018)
Slab dip angle	α_d	Slab2 (Hayes et al., 2018)
Crustal thickness	Tc	Crust1 (Laske et al., 2013)
Distance along trench	D	Distance from the northern edge of the trench (based on the projected position of volcanoes along the trench)
Obliquity	O	Deviation from trench-perpendicular convergence (R. D. Müller et al., 2016)
Convergence velocity	Rc	Trench-normal component of the relative velocity vector (R. D. Müller et al., 2016)
Age of subducting plate	A	Extrapolated from R. D. Müller et al. (2008)

areas where the slab is torn (e.g., Pesicek et al., 2012; Rosenbaum et al., 2018). However, for the purpose of defining SGAM, the Slab2 model provides a first-order approximation that allows us to detect general patterns in the spatial distribution of arc volcanoes. The geometry of the Andean slab shown by the Slab2 model is broadly similar to that inferred from seismic tomography (e.g., Chen et al., 2019; Portner et al., 2020).

The volcanoes considered here are those listed as Holocene volcanoes in the database of the Global Volcanism Program (2013) and are situated less than 200 km from the edge of the surface projection of the South American slab (Hayes et al., 2018) (Figure 1). The total number of volcanoes that meet these criteria is 165. Whole-rock geochemical data for these volcanoes are taken from the GeoROC database (<http://georoc.mpcn-mainz.gwdg.de/georoc>), manually scrutinized to minimize errors and inaccuracies, and complemented by additional published data. The complete dataset (Supporting Information, Table S1) consists of a total of 4688 whole-rock major and trace element analyses from 124 volcanoes. While most of these analyses are conducted on Holocene volcanic products, it is noted that many volcanoes in the list have experienced a longer eruption history during the Quaternary. Therefore, analyses from these volcanoes may also represent Pleistocene eruptions.

In addition to the available geochemical data, a range of other parameters are assigned to each volcano (Table 1). The depth of the slab (Hs) and the slab dip angle (α_d) are calculated for each volcano based on the Slab2 model. The parameter α_d represents the slab dip angle beneath each volcano (not the mean slab dip angle perpendicular to the trench). Crustal thickness (Tc) for each volcano is extrapolated from the Crust1.0 dataset (Laske et al., 2013). To allow spatial analysis along strike of the subduction zone, each volcano was projected to the plate boundary of Bird (2003) along a great circle that is tangential to the relative velocity vector at the volcano. Plate velocities are from R. D. Müller et al. (2016). Using these projections, we assign values for each volcano for: (1) the distance along the trench (from north to south); (2) the plate convergence obliquity (deviation from trench-perpendicular convergence); (3) the convergence velocity (trench-normal component of the relative velocity vector); and (4) the age of the subducting plate at the trench (based on R. D. Müller et al., 2008).

3. Spatial Variability

The list of 165 Holocene volcanoes in South America and their corresponding parameters is presented in Table S2. Below, we discuss along-strike variations in the distribution of the volcanic arc using the subduction parameters assigned for each volcano.

3.1. Density Along Strike

The density of volcanoes, calculated along the strike of the plate boundary, is variable (Figure 2a). The most prominent feature is the clustering of arc volcanism in three segments known as the Northern, Central, and Southern Andean Volcanic zones. These arc segments are separated by two broad volcanic gaps, the ~1600 km “Peru” gap and ~700 km “Chile” gap, that coincide with areas of flat slab and ridge subduction

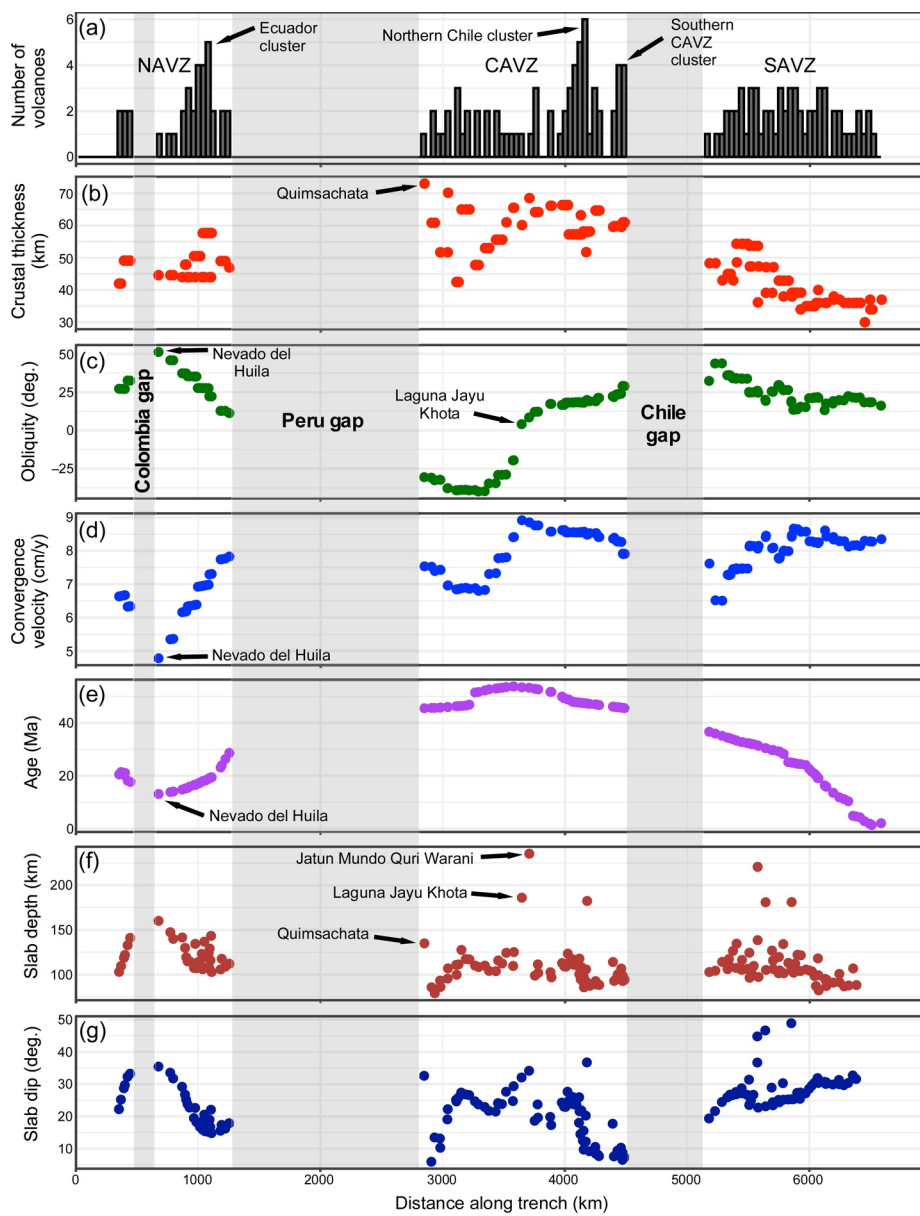


Figure 2. (a) Density of volcanoes (calculated for bin width of 40 km) projected along the trench, highlighting regions of volcanic clusters and gaps. CAVZ, Central Andean Volcanic Zone; NAVZ; Northern Andean Volcanic Zone; SAVZ, Southern Andean Volcanic Zone. (b) Along-strike variations in crustal thickness (calculated at the location of each volcano). (c) Along-strike variations in obliquity (deviation from trench-perpendicular convergence) calculated at the projected plate boundary location of each volcano; (d) Along-strike variations in the trench-normal component of the relative convergence velocity vector, calculated at the projected plate boundary location of each volcano; (e) Along-strike variations in the age of the subducting plate, calculated at the projected plate boundary location of each volcano; (f) Along-strike variations in slab depth (calculated at the location of each volcano); (g) Along-strike variations in slab dip angle (calculated at the location of each volcano).

(Figures 1 and 2) (McGeary et al., 1985; Sillitoe, 1974). A third, narrower, gap (the ~230 km long “Colombia” gap) occurs in the Northern Andean Volcanic Zone (Figure 2a). The average spacing of volcanoes in the Northern, Central, and Southern Andean Volcanic zones is 26, 25 and 22 km, respectively. Areas with high densities of volcanoes are the Ecuador cluster (corresponding to volcanoes at latitudes 0°–1°S), northern Chile cluster (latitudes 23°–24.5°S), and southern Central Andean Volcanic Zone cluster (latitudes 26.5°–27°S; Figure 2a).

3.2. Changes in Crustal Thickness

The crust underlying Andean volcanoes shows pronounced changes in thickness along strike (Figure 2b). In the Northern Andean Volcanic Zone, the average crustal thickness is 48.9 km ($\sigma = 5.1$ km), with the maximum crustal thickness (~57 km) associated with some of the volcanoes in the Ecuador cluster. The crust is substantially thicker in the Central Andean Volcanic Zone (average $T_c = 59.5$ km; $\sigma = 6.3$ km). Moreover, volcanoes in the northern Central Andean Volcanic Zone are underlain by a much broader range of crustal thicknesses, ranging from 42.5 km to >70 km. In the Southern Andean Volcanic Zone, the average crustal thickness is 41.5 km ($\sigma = 6.6$ km) with a general thinning of the crust from north (40–55 km) to south (30–35 km).

3.3. Changes in Subduction Kinematics

The curvature of the plate boundary and its angular relationship relative to the plate velocity vector (Figure 1) gives rise to along-strike variations in the subduction obliquity (Figure 2c). Nearly all Andean volcanoes are underlain by oblique subduction, with the relative convergence vector oriented clockwise relative to the trench (facing landward, shown by negative obliquity in Figure 2c) in the northern Central Andean Volcanic Zone, and counterclockwise (i.e., positive obliquity in Figure 2c) in the Northern and Southern Andean Volcanic zones and southern Central Andean Volcanic Zone. Orthogonal subduction occurs only in the middle of the Central Andean Volcanic Zone (Bolivian Orocline; Figure 1), opposite Laguna Jayu Khota. The volcano that corresponds to the maximum obliquity (>50°) is Nevado del Huila in the Northern Andean Volcanic Zone.

Calculations of the convergence velocity (trench-normal component of the relative velocity vector) show along-strike variations that may correspond to changes in the density of volcanoes (Figure 2a, d). The lowest velocity (4.8 cm/y) coincides with Nevado del Huila, immediately south of the Colombia volcanic gap. Farther south in the Northern Andean Volcanic Zone, the convergence velocity gradually increases to >7 cm/y. The volcanic clusters in the Central Andean Volcanic Zone (northern Chile and southern Central Andean Volcanic Zone clusters; Figure 2a) coincide with areas where the convergence velocity is relatively high (>8 cm/y; Figure 2d). In the Southern Andean Volcanic Zone, the convergence velocity increases from north to south (Figure 2d).

Along-strike variations in the age of the subducting lithosphere (Figure 2e) are particularly prominent in the Northern and Southern Andean Volcanic zones. The youngest lithosphere subducting in the Northern Andean Volcanic Zone occurs in the area of Nevado del Huila (~13 Ma), with older lithosphere occurring north and south of this volcano. In the Southern Andean Volcanic Zone, the lithosphere becomes progressively younger from north (>35 Ma) to south (<2 Ma). The oldest lithosphere, ranging from ~54 to ~45 Ma, is subducting opposite the Central Andean Volcanic Zone.

3.4. Location of Volcanoes Relative to the Slab

Relationships between volcanoes and slab structure can be considered based on the inferred depth and dip angle of the slab beneath each volcano (Figures 2f, g and 3). These parameters reveal spatial patterns associated with (1) along-strike variations relative to slab contours; (2) along-strike variations relative to the slab dip angle; (3) anomalous slab depth beneath individual volcanoes; and (4) absence of slab beneath individual volcanoes.

3.4.1. Along-Strike Variations Relative to Slab Contours

The volcanic arc in the northernmost part of the Northern Andean Volcanic Zone (Colombia) is not parallel to the Slab2 contours, but instead delineates a roughly sinusoidal trend (Figures 2f and 3b). In detail, the slab depth increases from ~110 km beneath Romeral and Cumbal to a maximum depth of 160 km beneath Nevado del Huila, at the southern edge of the Colombia volcanic gap (Figure 3b). Farther south, in Ecuador, most volcanoes are aligned parallel to the slab contours at depths of 100–120 km (Figure 3b).

The northernmost Central Andean Volcanic Zone is another area where slab contours are not parallel to the alignment of volcanoes (Figure 3c). Moving southwards from the southern edge of the Peru flat

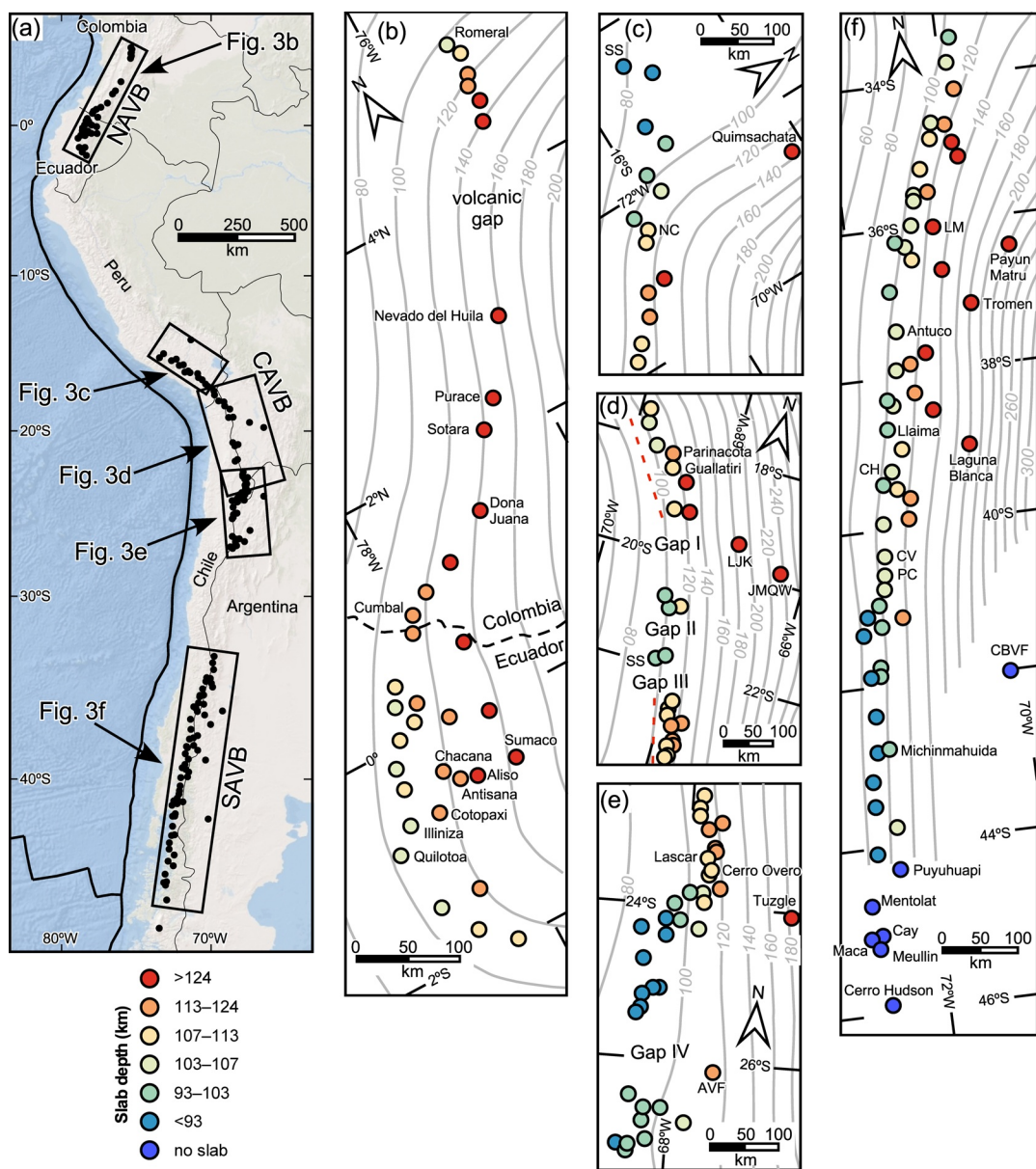


Figure 3. Maps showing locations of volcanoes relative to slab contours (gray lines with numbers indicating depth in km; after Hayes et al., 2018). Specific volcanoes that are mentioned in the text are labeled. The color code corresponds to the depth of the slab beneath each volcano (Table S2). (a) Location map. CAVZ, Central Andean Volcanic Zone; NAVZ; Northern Andean Volcanic Zone; SAVZ, Southern Andean Volcanic Zone. (b) Northern Andes. (c) Northernmost Central Andes. NC, Nevado Chachani; SS, Sara Sara. (d) Central part of the Central Andes (Bolivian Orocline). The dashed red lines highlight the change in the strike orientation of the volcanic arc, from 145° in the north to 165° in the south. JMqw, Jatum Mundo Quri Warani; LJK, Laguna Jayu Khota; SS, San Pedro-San Pablo. (e) Southern part of the Central Andes. AVF, Antofagasta Volcanic Field. (f) Southern Andes. CBVF, Crater Basalt Volcanic Field; CH, Caburgua-Huelemolle; CV, Carran-Los Venados; LM, Laguna del Maule; PC, Puyehue-Cordon Caulle.

slab segment (Figure 3c), the slab depth increases from less than 80 km (Sara Sara) to ~ 110 km (Nevado Chachani). In the central part of the Central Andean Volcanic Zone, most volcanoes are aligned parallel to the slab contours (100–120 km depths), but between latitudes 19.2°S and 22.5°S , this chain of volcanoes is interrupted by three volcanic gaps (Gaps I, II, and III in Figure 3d). In the southern Central Andean Volcanic Zone, the arrangement of Holocene volcanoes shows a prominent kink, with volcanoes north and south of latitude 24°S situated above a slab depth of ~ 110 and ~ 90 km, respectively (Figure 3e). In the area

of the kink, a ~100 km segment of the volcanic arc is oriented at a high angle relative to the slab contours (Figure 3e). Another volcanic gap (Gap IV in Figure 3e) occurs around latitude 26°S.

In the Southern Andean Volcanic Zone, most volcanoes are aligned parallel to the slab contours (depths 80–120 km; Figure 3f). However, a general decrease in the slab depth is recognized from north to south, with a subtle kink at around latitude 41°S (Figures 2f and 3f).

3.4.2. Variations in the Slab Dip Angle

Along-strike variations in the slab dip angle (Figure 2g) show a gradual decrease in the slab dip angle toward the Peru and Chile volcanic gaps. At the northern and southern edges of the Central Andean Volcanic Zone, the slab dip angle is <10°. The Colombia volcanic gap, in contrast, is not associated with a particularly low slab dip angle, with nearby volcanoes underlain by a >30° dipping slab (Figure 2g).

3.4.3. Slab Depth

A number of Holocene volcanoes in South America occur in areas where the slab is anomalously deep (relative to “typical” depths of 124 ± 38 km; Stern, 2002). In the Northern Andean Volcanic Zone, the slab beneath Dona Juana, Sotara, Purace, and Nevado del Huila is relatively (but not anomalously) deep at 140–160 km (Figure 3b). Farther south, Sumaco is farthest from the frontal arc, at a nominal slab depth of ~145 km (Figure 3b), albeit in an area where the slab is considered to be torn (Rosenbaum et al., 2018).

In the northernmost Central Andean Volcanic Zone, Quimsachta occurs off-axis relative to the rest of the Holocene volcanoes, at a slab depth of ~135 km (Figure 3c). The strike of the Central Andean Volcanic Zone changes from 145° to 165° at around latitude 20°S, coinciding with a ~175 km gap in arc-front volcanism (Gap I in Figure 3d) and the occurrence of two volcanoes (Laguna Jayu Khota and Jatun Mundo Quri Warani) that are located where the slab is anomalously deep (depths of 190 and 230 km, respectively). In the southern Central Andean Volcanic Zone, Tuzgle (northwestern Argentina) is underlain by a portion of slab that is ~180 km deep (Figure 3e). The position of Tuzgle, at latitude 24°S, coincides with the prominent kink in the frontal arc of the Central Andean Volcanic Zone.

The locations of three volcanoes in the Southern Andean Volcanic Zone corresponds to anomalous slab depths (Figure 3f). The slab underlying Payun Matru is ~220 km deep. Farther south, Tromen and Laguna Blanca both occur above the 180 km slab contours, marking the edge of two parallel chains of NW–SE volcanoes at latitude 36°–39°S (Figure 3f).

3.5. Absence of Slab

All Holocene volcanoes in the Southern Andean Volcanic Zone south of latitude 44.2°S are located in a region that the Slab2 model suggests may not be underlain by a subducting slab (Figure 3f). Situated closest to the slab edge (<200 km) are Puyuhuapi, Mentolat, Cay, Maca, Meullin, and Cerro Hudson (Figure 3f). Farther north, the Crater Basalt Volcanic Field is also positioned beyond the edge of the slab, more than 180 km east of the volcanic arc.

4. Geochemical Variability

The vast majority of volcanic rocks in the Andes are basaltic andesite, andesite, dacite and rhyolite belonging to the calc-alkaline series (Figure 4). However, some volcanoes—particularly those that occur where the slab is relatively deep (or absent)—are characterized by anomalous compositions. The widespread occurrence of relatively low total alkali rocks (basalt to rhyolite) represents normal arc melting at the typical slab depths of 80–110 km. Intermediate compositions (andesite and trachy-andesite) are much more prevalent in the northern and central segments, whereas basalt and basaltic andesite dominate in the south (Figure 4). Broadly, this observation can be explained by crustal thickness variations (Figure 2b), with the least differentiated magmas (basalts) occurring where the crust is thinnest (Southern Andean Volcanic Zone).

A number of volcanic samples, particularly from the Northern Andean Volcanic Zone; and Southern Andean Volcanic Zone, are associated with alkaline and ultra-alkaline compositions. Sumaco phonolite series lavas range from basanite/tephrite to tephri-phonolite (Figure 4a) (Garrison et al., 2018). In the Southern

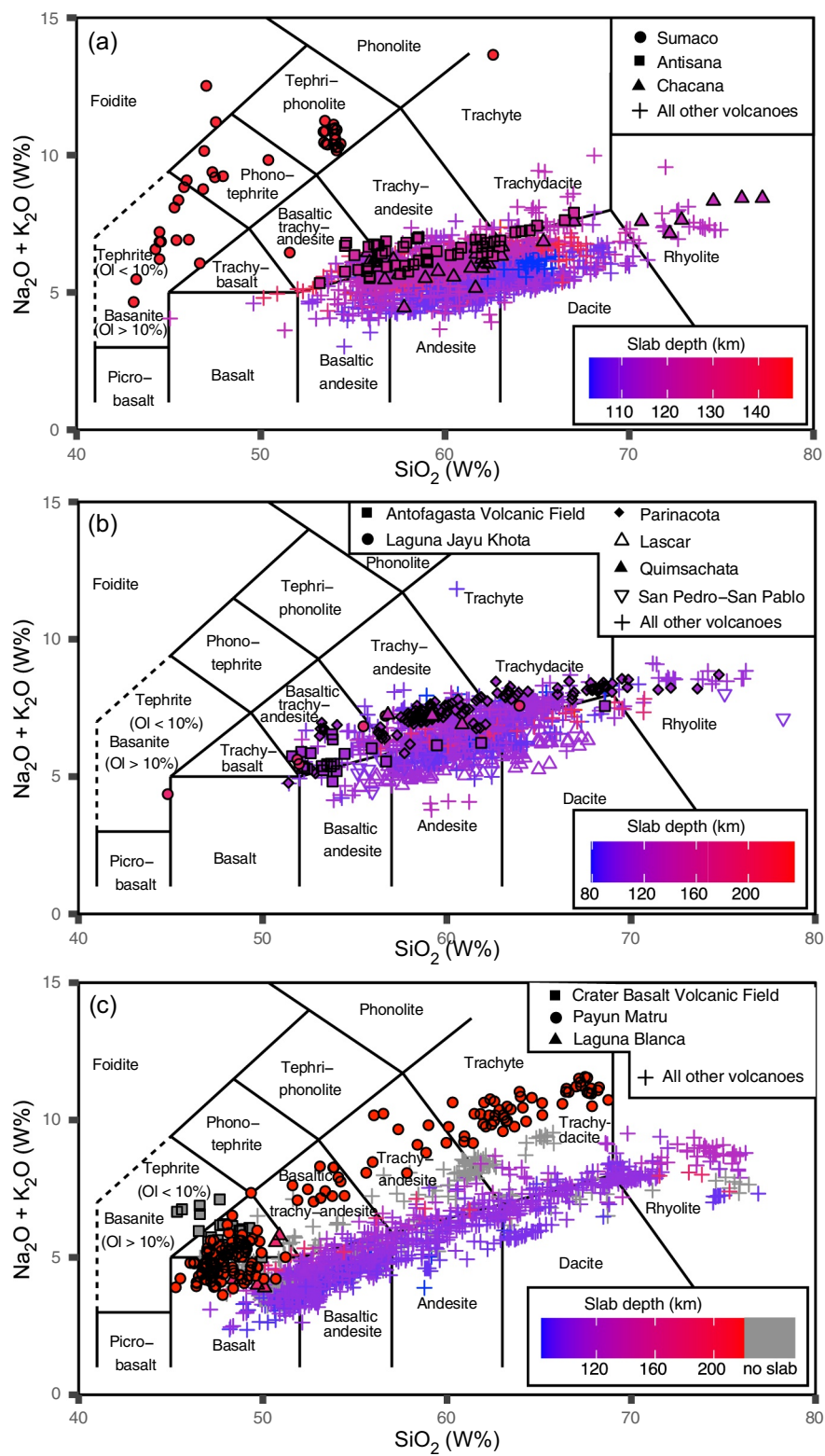


Figure 4. Total alkali versus silica classification diagrams (Le Bas et al., 1986) for Holocene volcanoes in the (a) Northern Andean Volcanic Zone; (b) Central Andean Volcanic Zone; and (c) Southern Andean Volcanic Zone. The color scale is coded for the depth of the slab below each volcano (see Table S2) and the different symbols highlight specific volcanoes that are discussed in the text.

Table 2

Criteria Used to Calculate the Geochemical Anomaly Score for Whole-Rock Analyses

Criterion	Geochemical signature	Score
Degree of fractionation	$\text{SiO}_2 < 62 \text{ wt.\%}$ $5 < \text{MgO} < 10 \text{ wt.\%}$	Score 0 assigned to analyses that do not pass these screening filters.
Absence of metasomatic fluid contributions	$\text{Ba/La} < 30$ $\text{Ba/Th} < 200$ $\text{Ce/Pb} > 6$	One point assigned for each criterion (maximum score = 8).
Degree of melting	$\text{K}_2\text{O} + \text{Na}_2\text{O} > 5 \text{ wt.\%}$	
Slab melt component	$\text{Nb/Y} > 0.6$	
Depth of melting	$\text{La/Yb} > 25$	
Absence of slab sediments	$\text{Th/Ce} < 0.1$ $\text{Th/Nb} < 0.2$	

Andean Volcanic Zone, basanite/tephrite and trachybasalt compositions are found in rocks from the Crater Basalt Volcanic Field. Rocks from Payun Matru and Laguna Blanca are characterized by alkaline compositions spanning trachybasalt to trachyte (Figure 4c).

To further understand geochemical anomalies in volcanic arcs, we developed a scoring system that assesses the deviation of a specific sample (or group of samples) from typical arc-related geochemical signatures. The scoring system is based on a series of geochemical indices that provide insights into the degree of fractionation, the role of metasomatic fluids in melt generation, the degree of melting, the depth of melting, and the involvement of subducted sediments and slab-derived melts (Table 2). Score rankings range from 0 to 8, with the lowest rank representing a typical arc-related volcanic rock (or a fractionated rock, and therefore excluded), and the highest rank indicating a strongly anomalous mafic to intermediate composition.

Geochemical anomaly scores were calculated for each individual entry in our database (Supporting Information Table S1) and for each volcano (Supporting Information Table S2). A score of 0 is assigned where none of the analyses from a volcano pass both screening filters for the degree of fractionation ($\text{SiO}_2 < 62 \text{ wt.\%}$ and $5 < \text{MgO} < 10 \text{ wt.\%}$; Table 2). Of the remaining analyses in the dataset, one point is added for each additional geochemical criterion met (Table 2). Whilst the fractionation filter is applicable in the Andes, we acknowledge that hot-slab subduction zones (e.g., SW Japan Arc, Kimura et al., 2014) can produce intermediate to evolved magmas with moderate SiO_2 and MgO. In such cases, Mg# may be considered a more appropriate filter.

4.1. Degree of Fractionation

The ability to recognize anomalous melting in arc settings is necessarily hampered by magmatic differentiation processes, which generate magmas that are strongly fractionated or contaminated by crustal components. To obtain a better insight into the origin of the melt, we first assess the degree of magma differentiation using SiO_2 and MgO screening tests. Fractionated magmas are characterized by higher concentrations of SiO_2 ($\text{SiO}_2 > 62 \text{ wt.\%}$) and lower MgO contents ($\text{MgO} < 5 \text{ wt.\%}$). Accordingly, analyses with $\text{SiO}_2 > 62 \text{ wt.\%}$ and $\text{MgO} < 5 \text{ wt.\%}$ are excluded from the scoring system (Figure 5). We also exclude analyses with $\text{MgO} > 10 \text{ wt.\%}$ as they may represent cumulates (Streck & Leeman, 2018; Ubide et al., 2014). Out of the 4688 analyses, 3938 (84%) do not pass the SiO_2 and/or MgO tests (red dots in Figure 5). These analyses are automatically assigned a geochemical anomaly score of 0.

Nearly all analyses that pass the MgO test also pass the SiO_2 test (blue dots in Figure 5). However, a large number of analyses that pass the SiO_2 test do not pass the MgO test (red dots below the $\text{SiO}_2 = 62 \text{ wt.\%}$ threshold in Figure 5a). This indicates that the MgO screening test provides a stricter constraint on our scoring system, which effectively limits scores of ≥ 1 to mafic or low-silica intermediate rocks ($\text{SiO}_2 < 55 \text{ wt.\%}$; Figure 5a).

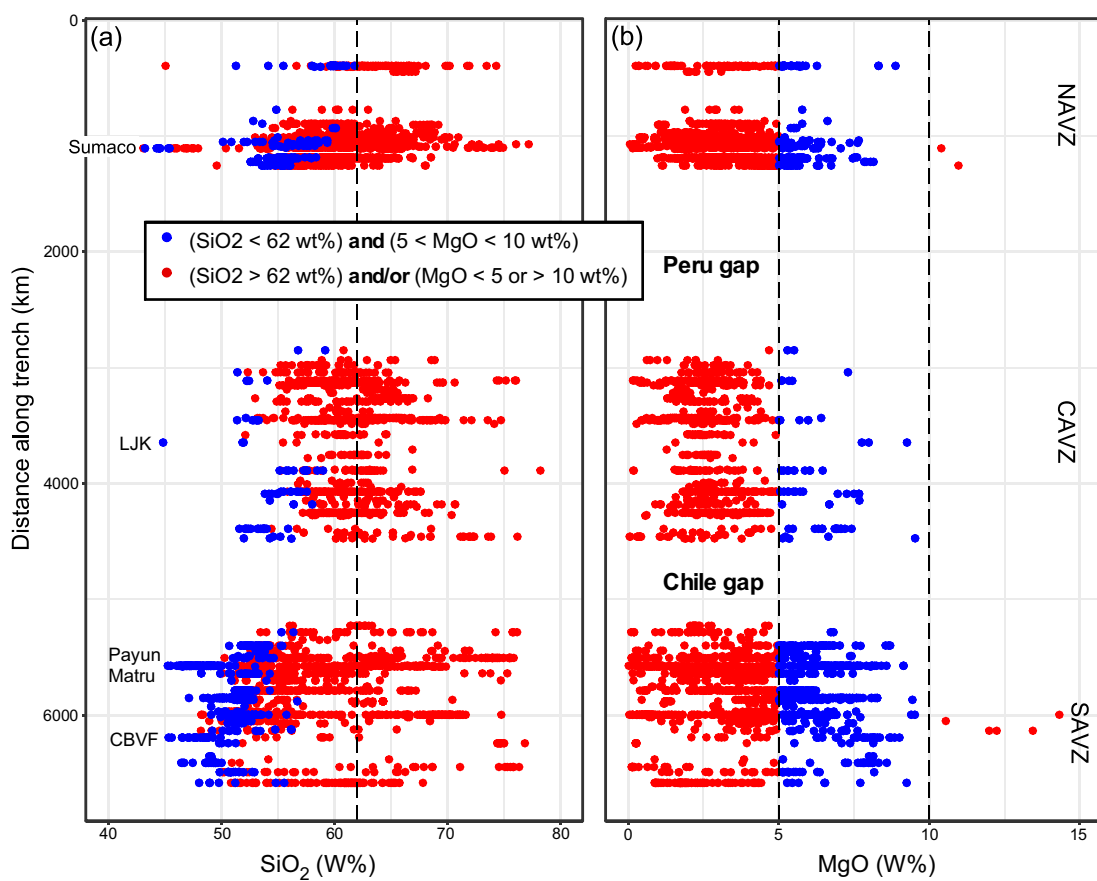


Figure 5. Variations in (a) SiO_2 and (b) MgO along strike. Blue dots correspond to data that pass both screening filters for the degree of fractionation (i.e., $\text{SiO}_2 < 62 \text{ wt\%}$ and $5 < \text{MgO} < 10 \text{ wt\%}$), thus representing relatively less evolved magmas. Red dots correspond to data that fail one or both screening tests. CAVZ, Central Andean Volcanic Zone; CBVF, Central Basalt Volcanic Field; LJK, Laguna Jayu Khota; NAVZ; Northern Andean Volcanic Zone; SAVZ, Southern Andean Volcanic Zone.

Altogether, analyses from 72 Holocene volcanoes pass the SiO_2 and MgO screening tests. Data discussed in the following sections and plotted in Figures 6 and 7, are restricted to those analyses (blue dots in Figure 5). Along the strike of the Andean belt, we recognize that mafic rocks are most abundant in the Southern Andean Volcanic Zone and are relatively scarce in the Central Andean Volcanic Zone (Figure 5). This pattern likely reflects variations in crustal thickness (see Section 5.1). The lowest SiO_2 values ($\text{SiO}_2 < 46 \text{ wt\%}$) are recognized at Sumaco, Laguna Jayu Khota (LJK), Payun Matru, and Crater Basalt Volcanic Field (CBVF). In these localities, the occurrence of very low SiO_2 and high MgO rocks indicate that volcanism was derived from a particularly primitive melt, and/or underwent limited differentiation during ascent.

4.2. Role of Dehydration Fluids

The generation of melts in “typical” arc systems is facilitated by the contribution of dehydration fluids that originate in the subducting slab (e.g., Gill & Williams, 1990). Therefore, arc magmas are expected to be enriched in fluid-mobile large ion lithophile elements (LILE), such as Ba and Pb, relative to fluid-immobile high field strength elements (HFSE), such as Th and rare earth elements (REE; e.g., La and Ce). Here we use elemental ratios of Ba/La and Ba/Th to assess the contribution of slab-derived fluids (Pearce & Peate, 1995; Turner et al., 1997), with the assumption that volcanic rocks with anomalously low values of Ba/La (<30) and Ba/Th (<200) originated from a melt source that was not strongly affected by the presence of slab-derived fluids. Similarly, Ce/Pb values >6 are also inferred to reflect negligible addition of Pb-rich subduction derived fluids (Brenan, Shaw, Ryerson, 1995a). We emphasize, however, that in the absence of Pb isotope data, a sedimentary control on the value of Ce/Pb cannot be excluded. The threshold values selected for the

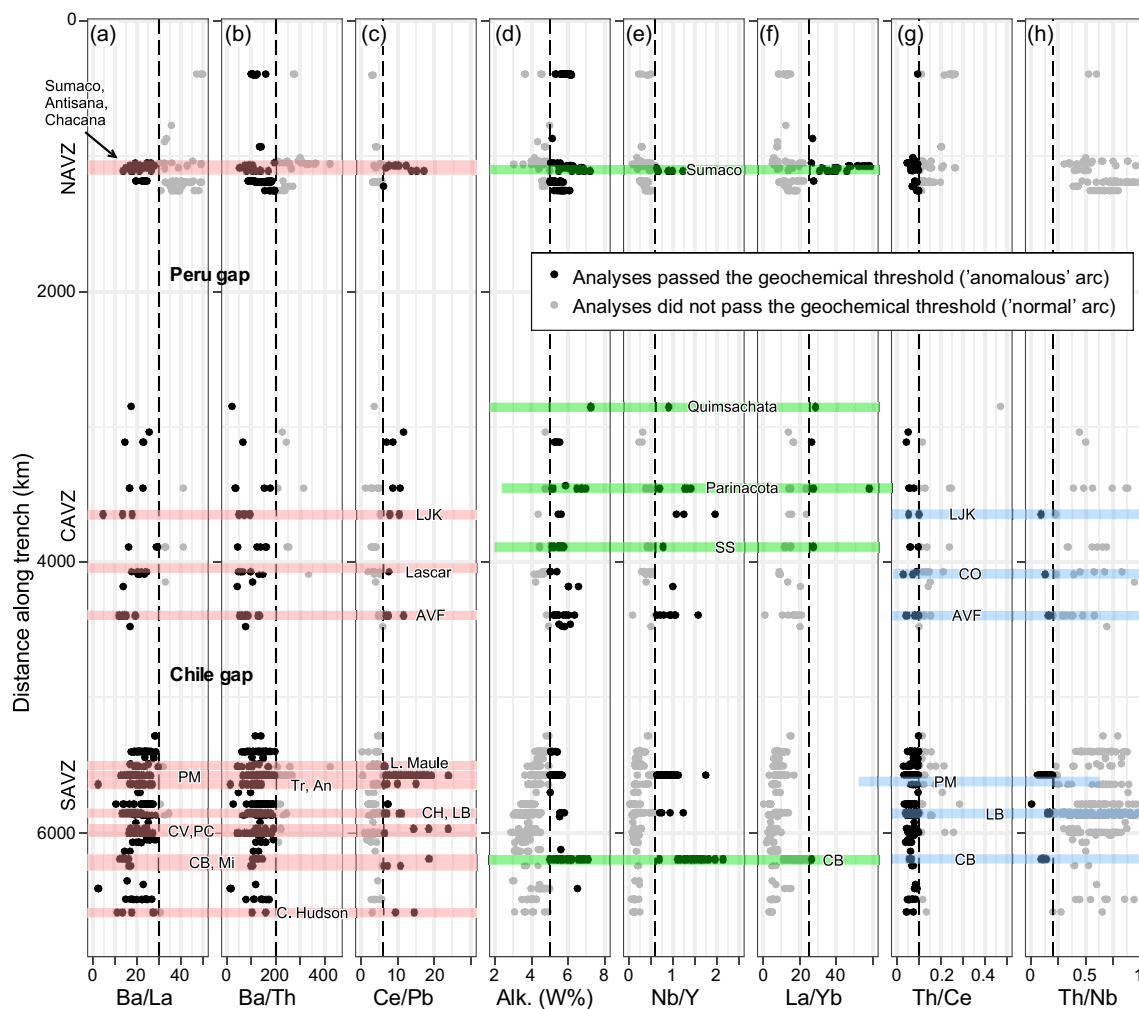


Figure 6. Geochemical variations along strike for less evolved samples that pass the SiO_2 and MgO screening tests (see Figure 5). Red bars correspond to locations along strike that show evidence for a reduced contribution of metasomatic fluids to the source ($\text{Ba/La} < 30$, $\text{Ba/Th} < 200$, and $\text{Ce/Pb} > 6$). Green bars represent locations with evidence for lower degrees of partial melting ($\text{K}_2\text{O} + \text{Na}_2\text{O} > 5$ wt.-%), a slab melt contribution ($\text{Nb/Y} > 0.6$), and an increased depth of melting within the garnet stability field ($\text{La/Yb} > 25$). Blue bars indicate locations with low subducted sediment input ($\text{Th/Ce} < 0.1$, $\text{Th/Nb} < 0.2$). An, Antuco; AVF, Antofagasta Volcanic Field; CAVZ, Central Andean Volcanic Zone; CB, Crater Basalt Volcanic Field; CH, Caburgua-Huelemolle; C. Hudson, Cerro Hudson; CO, Cerro Otero; CV, Carran-Los Venados; LB, Laguna Blanca; L. Maule, Laguna del Maule; LJK, Laguna Jaya Khota; Mi, Michinmahuida; NAVZ, Northern Andean Volcanic Zone; PC, Puyehue-Cordon Caulle; PM, Payun Matru; SAVZ, Southern Andean Volcanic Zone; SS, San Pedro-San Pablo; Tr, Tronem.

present study are largely based on average “arc front” values compiled for the Northern Andean Volcanic Zone (Rosenbaum et al., 2018). Ambiguities may arise in subduction regimes dominated by clay-rich subducted sediments (Ba/La), in equatorial arc systems with significant carbonate and marine barite in the sediment pile (Ba/Th), and due to the nature of detrital mineral phases in downgoing sediments (HFSE) (Plank & Langmuir, 1998). Accordingly, global inter-arc variability would require a case-by-case geochemical assessment of threshold values for scoring criteria, in accordance with available data for local subduction input reservoirs and the erupted rock record.

Most mafic and intermediate samples (i.e., those that pass the SiO_2 and MgO screening tests) are characterized by relatively low values of Ba/La and Ba/Th (Figure 6a, b), indicating a relatively minor role of slab-derived fluids in these volcanoes. These elemental ratios are particularly low in the Southern Andean Volcanic Zone. In contrast, some mafic-intermediate rocks from the Northern Andean Volcanic Zone have higher values of Ba/La and Ba/Th , indicating a “typical arc” fluid-assisted melting process (Figure 6a, b). The third elemental ratio used to assess slab fluids, Ce/Pb , represents the most restrictive test (i.e., many analyses that pass the other two tests fail this test; Figure 6a–c).

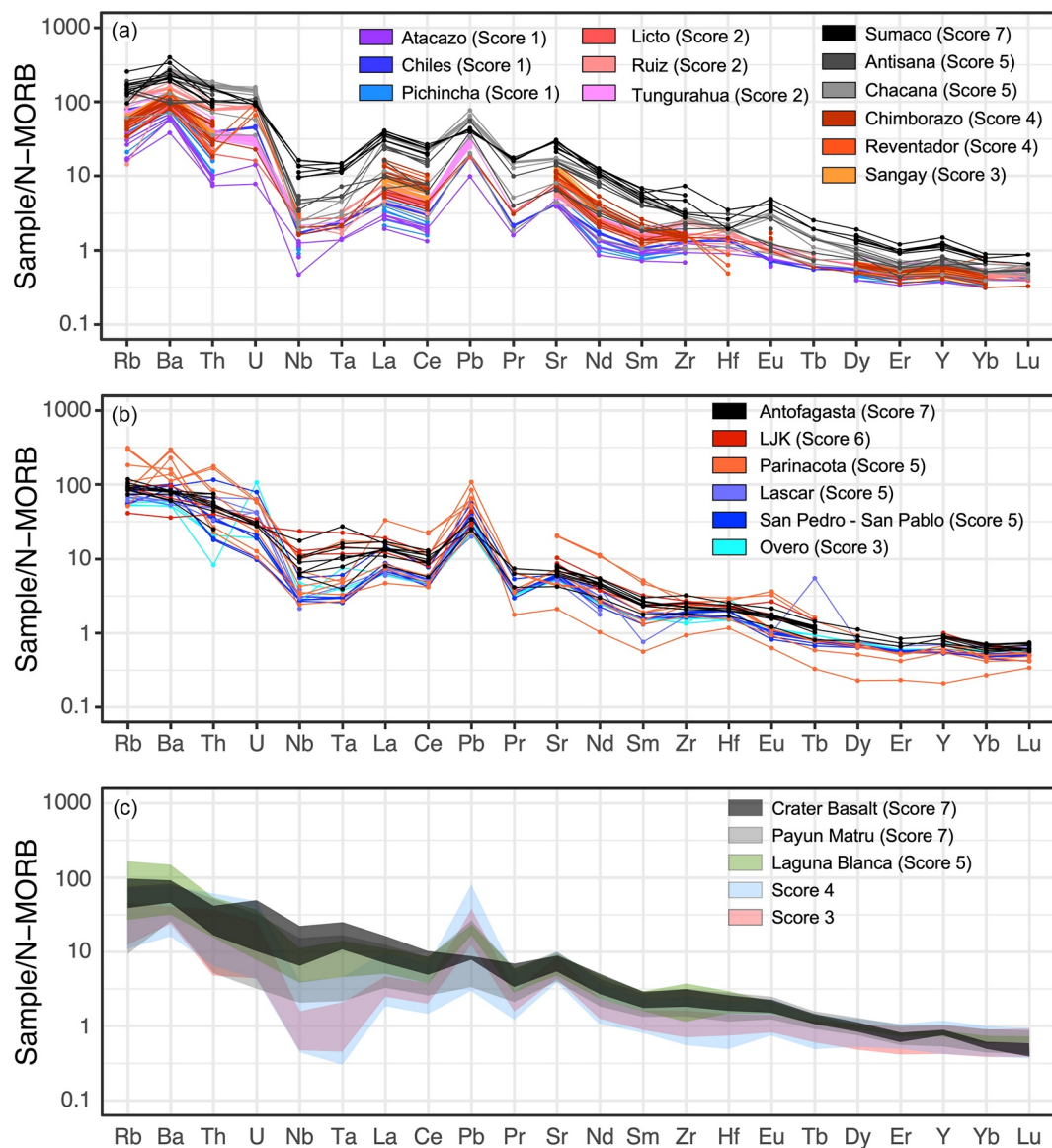


Figure 7. Multi-element diagrams normalized relative to normal mid-oceanic ridge basalt (N-MORB, Sun & McDonough, 1989) for all data that pass the silica and magnesium screening tests. (a) Northern Andean Volcanic Zone; (b) Central Andean Volcanic Zone; (c) Southern Andean Volcanic Zone. Note that there are several low score (<3) volcanoes in the Central and Southern Andean Volcanic zones, but none of them had sufficient analyses to meet the minimum number of analyses requirement ($n = 3$) for inclusion in the multi-element diagrams.

Using the combined three tests, we recognize a cluster of “anomalous” compositions in the Northern Andean Volcanic Zone (highlighted in red in Figure 6a–c), which represent samples from Sumaco, Antisana, and Chacana (for map locations of the specified volcanoes, see Figure 3). Indeed, relative to other volcanoes in the Northern Andean Volcanic Zone, samples from Sumaco, Antisana and Chacana show lesser degrees of enrichment in fluid mobile elements (e.g., Ba, U, Pb, and Sr) and depletion in fluid immobile elements (e.g., Nb and Ta; Figure 7a). The lower fluid input in these volcanoes, and particularly in Sumaco, is also evident by the relatively low positive Pb anomaly (in comparison with the more pronounced Pb anomaly, relative to neighboring Ce and Pr, recognized in other volcanoes; Figure 7a).

Data from the Central Andean Volcanic Zone are dispersed (Figures 6 and 7b), with only few analyses passing the SiO_2 and MgO screening tests. Analyses that pass all the three tests for the role of dehydration

fluids (thus indicating “anomalous” compositions) are from Laguna Jayu Khota, Lascar, and Antofagasta Volcanic Field (Figure 6a–c).

A relatively large number of analyses from the Southern Andean Volcanic Zone pass all three tests for the role of dehydration fluids. These include analyses from Laguna del Maule, Payun Matru, Tromen, Antuco, Laguna Blanca, Caburgua-Huelemolle, Carran-Los Venados, Puyehue-Cordon Caulle, Crater Basalt Volcanic Field, Michinmahuida, and Cerro Hudson (Figures 3f and 6a–c). The normalized multi-element diagrams (Figure 7c) further highlight the reduced role of subduction-related fluids in Crater Basalt Volcanic Field, Payun Matru, and Laguna Blanca. Relative to analyses of other rocks from the Southern Andean Volcanic Zone, samples from these three volcanoes do not show the same level of enrichment in Pb and marked depletions in Nb and Ta (Figure 7c).

4.3. Degree of Melting, Slab Melt Component, and Depth of Melting

Typical arc sources are inferred to melt by ~15% (Plank & Langmuir, 1998) at characteristic depths of ~75 km (Tatsumi et al., 1986). Under these conditions, magmas are expected to have total alkalis ($K_2O + Na_2O$) of < 5 wt.%. In marked contrast, we consider that alkaline volcanic rocks ($K_2O + Na_2O > 5$ wt.%) with values of Nb/Y (>0.6) and La/Yb (>25) reflect lower degrees of melting (<5%) at greater depths (>80 km), unassisted by fluid metasomatism. Indeed, elevated Nb/Y and La/Yb have been inferred to record a component of HFSE-enriched slab-derived melt generated in the garnet stability field. This metasomatic agent is inferred to have facilitated melting of the overlying ambient mantle (e.g., Hoffer et al., 2008; Rosenbaum et al., 2018).

Of the rocks that pass the SiO_2 and MgO tests, only a small number of analyses pass all three criteria for anomalous degree and depth of melting (green bars in Figure 6d–f). In the Northern Andean Volcanic Zone, such “anomalous” analyses are only from Sumaco. In the Central Andean Volcanic Zone, a few analyses from Quimsachata, Parinacota, and San Pedro-San Pablo pass all three criteria. In the Southern Andean Volcanic Zone, these three criteria are met only in one sample, from Crater Basalt Volcanic Field (Figure 6d–f).

4.4. Sediment Input

Melt generation in convergent margin settings can incorporate a component of sediment input from the subducting slab (Plank & Langmuir, 1998). Such contributions have been shown to be characterized by enrichments in Th relative to LREE and HFSE, such as Nb and Ta. To track the contribution of sediment to the source we use Th/Ce and Th/Nb ratios (Hawkesworth et al., 1997; Plank & Langmuir, 1998). Assuming that anomalous arc magmas are not affected by sediment input, we consider threshold values of <0.1 for Th/Ce and <0.2 for Th/Nb to pass the sediment free test. However, as discussed previously, significant diversity exists in the lithological make-up of subducting sediments globally, so sediment indices for individual arc systems should be assessed independently.

The overwhelming majority of analyses that pass the SiO_2 and MgO tests also pass the Th/Ce test, but only a few analyses are below the threshold for the Th/Nb test (Figure 6g, h). None of the analyses from the Northern Andean Volcanic Zone pass both tests, indicating that the influence of sediment input during melting may be appreciable in this part of the Andean belt (Errázuriz-Henao et al., 2019). In contrast, low values of both Th/Ce and Th/Nb (blue bars in Figure 6g, h) are found in several volcanoes in the southern part of the Central Andean Volcanic Zone (Laguna Jayu Khota, Cerro Otero, Antofagasta Volcanic Field) and in the Southern Andean Volcanic Zone (Payun Matru, Llaima, Laguna Blanca, Crater Basalt Volcanic Field).

5. Discussion

5.1. Relationships Between Subduction Parameters and Geochemical Anomalies

Numerous factors can affect the geochemical composition of volcanic rocks including the composition of the sub-arc mantle, variable slab flux (relative fluid/sediment contributions and composition), subducting slab heterogeneities (slab age, thickness, surface temperatures, fracture zones, ridges), and overriding-plate heterogeneities (thickness, composition, stress regime). In addition, the criteria used to calculate

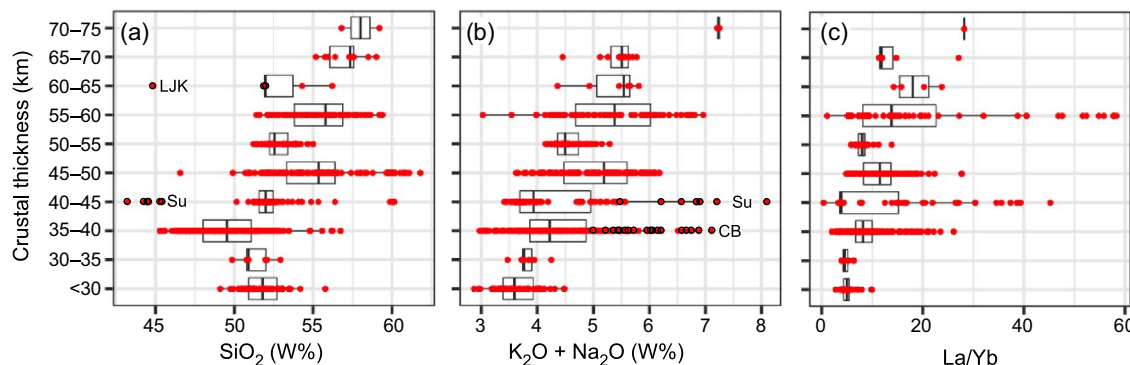


Figure 8. Relationships between crustal thickness and (a) SiO₂; (b) total alkalis; and (c) La/Yb. The complete plots are presented in Supporting Information Figure S1. Data plotted are only from analyses that pass the SiO₂ and MgO screening tests (Table 2). Each box shows the first and third quartiles (the 25th and 75th percentiles). The thick black line is the median. The horizontal black line extends to the largest and smallest values no further than 1.5 IQR from the box (where IQR is the distance between the first and third quartiles). Outliers appear beyond the horizontal lines. Bold circles highlight analyses from Crater Basalt Volcanic Field (CB), Laguna Jayu Khota (LJK), and Sumaco (Su).

the geochemical anomaly scores (Table 2) are also influenced by slab geometry (e.g., slab depth and dip angle), together with kinematic considerations (convergence rate and subduction obliquity). Using our dataset from the Andes, we explore the relationships between these parameters and the geochemical criteria employed here in order to better constrain the critical factors responsible for the generation of SGAM (Supporting Information Figures S1–S6).

Thicker crust results in enhanced magmatic differentiation, leading to magmas that are enriched in SiO₂ and incompatible elements (Farmer & Lee, 2017). This pattern is evident in the Andean arc, with volcanoes that are underlain by thicker crust generally showing SiO₂ enrichment relative to those underlain by thinner crust (Figure 8a). Two notable exceptions are Sumaco and Laguna Jayu Khota, which, relative to their crustal thicknesses (44 and 60 km, respectively), are anomalously mafic. In addition, a positive correlation between crustal thickness and total alkali content can be recognized (Figure 8b). Enhanced magmatic differentiation and the increased potential for crustal assimilation in thick crust are likely to increase the concentration of incompatible elements such as K. We note, however, that relative to their crustal thicknesses, some volcanoes (Sumaco, Crater Basalt Volcanic Field) display an anomalously high total alkali content. Previous studies have suggested that LREE/HREE fractionation (e.g., La/Yb) reflects residual garnet in the source (Drummond & Defant, 1990), which provides a proxy for depth of melting and may, in turn, be linked to crustal thickness (Mantle & Collins, 2008; Profeta et al., 2015). These relationships are somewhat apparent in our data, which show a general increase in the median value of La/Yb with increasing crustal thickness (Figure 8c).

Our analysis shows no clear relationship between the geochemical indices and the orientation of subduction relative to the trench (obliquity), convergence velocity, and age of the subducting slab (Figures S2–S4). Previous authors have suggested that faster convergence rates and minimal obliquity are instrumental in sustaining magmatic flux, thus affecting the potential to create larger eruptions (Hughes & Mahood, 2008; Sheldrake et al., 2020). While we are unable to fully test this hypothesis, we recognize that the area of maximum obliquity and minimum convergence velocity, near Nevado del Huila (Figure 2c, d), coincides with the location of the Colombia gap (Figure 2a). The calculated obliquity and convergence rate values at the center of the volcanic gap (latitude 3.5°N, longitude 75.5°) are 51.14° and 4.77 cm/y, respectively. This volcanic gap, unlike the Peru and Chile gaps, cannot be attributed to flat subduction (Figure 2g), thus raising the possibility that the absence of volcanism in the Colombia gap is partially driven by the high obliquity and/or the low convergence rate. In other words, the recognition that the volcanic gap partially overlaps with a change in the trench azimuth (which results in oblique subduction) raises the possibility that in this segment of the subduction zone, the magmatic flux generated by oblique subduction is too low to sustain substantial volcanism.

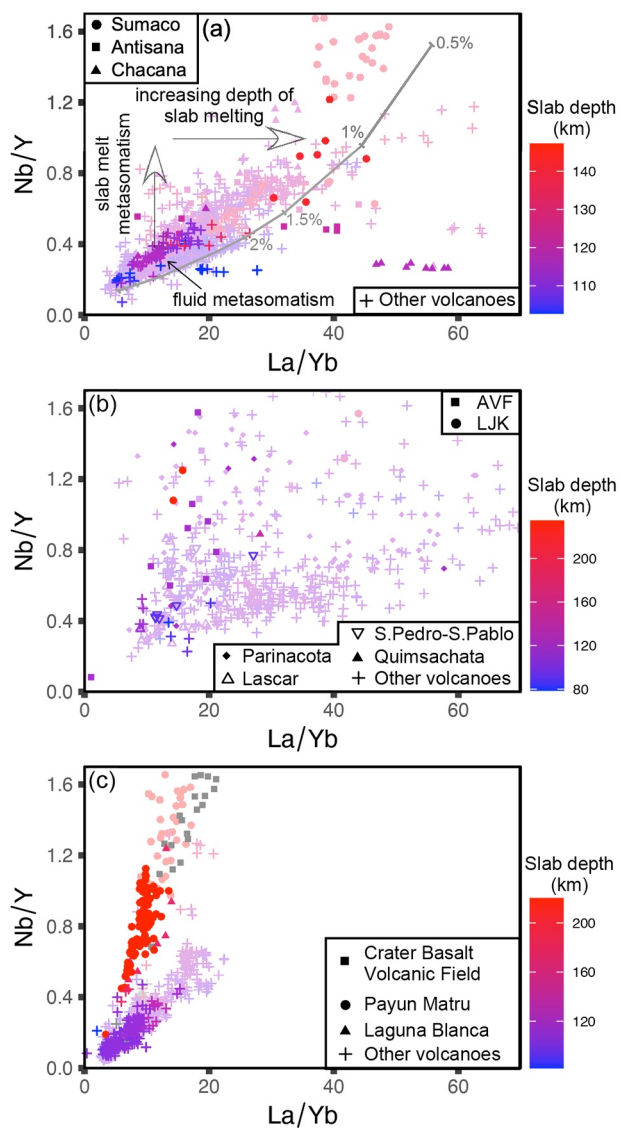


Figure 9. Nb/Y versus La/Yb diagrams for the (a) Northern Andes; (b) Central Andes; and (c) Southern Andes. The white arrows in (a) highlight trends from fluid-induced metasomatism (normal subduction) to more anomalous magmatism involving slab melt-induced metasomatism and/or an increase in the depth of slab melting (after Hoffer et al., 2008). The thick gray line indicates melting trajectories for an estimated Sumaco source (Rosenbaum et al., 2018) with tick marks indicating percent melting. The transparent symbols in the background refer to analyses that did not pass the SiO₂ and MgO screening tests (Table 2). AVF, Antofagasta Volcanic Field; LJK, Laguna Jayu Khota.

Establishing relationships between slab geometry (depth and dip) and the different geochemical indices is not straightforward (Figures S5 and S6). However, plotted on Nb/Y versus La/Yb diagrams, the data show that increasing slab depths are generally associated with higher values of Nb/Y and La/Yb (Figure 9). This behavior is best displayed in the Northern Andean Volcanic Zone (Figure 9a) and is likely linked to lower degrees of melting assisted by slab melt-induced metasomatism (Hoffer et al., 2008). Mafic and intermediate samples from volcanoes that are underlain by “typical” slab depths of 90–110 km, both in the Northern and Southern Andean Volcanic zones, have lower values of Nb/Y and La/Yb, which indicate higher degrees of melting typical of fluid-induced metasomatism (Figure 9a, c). Importantly, the data clearly highlight the anomalous behavior of Sumaco (Figure 9a), Payun Matru, Laguna Blanca and Crater Basalt Volcanic Field (Figure 9c), thus supporting the idea that these volcanoes do not reflect the release of metasomatic fluids from the subducting slab. Interestingly, data from the Northern Andean Volcanic Zone show a continuum from normal to anomalous compositions (e.g., Sumaco; Figure 9a), perhaps recording the transition from shallower fluid-fluxed melting to more anomalous compositions generated overlying a deeper slab and a tear (Rosenbaum et al., 2018). In contrast, data from the Southern Andean Volcanic Zone define two separate trends (Figure 9c), suggesting two separate, non-overlapping modes of melt generation (normal arc and anomalous). The anomalous trend indicates a strong slab melt component (high Nb/Y), but relatively low values of La/Yb (in comparison with the Northern Andean Volcanic Zone). This behavior might be attributed to the fact that the slab underlying the Southern Andean Volcanic Zone is relatively young (1–37 Ma; Figure 2e), and by inference hotter and therefore more likely to melt (e.g., Defant & Drummond, 1990). Additionally, enhanced buoyancy may promote melting of the slab at shallower depths (above the garnet stability field) at the slab edge or in areas where the slab is torn. The data from the Central Andean Volcanic Zone do not show a clear pattern (Figure 9b), possibly because of the greater crustal thickness and the loss of primary mantle signatures by magmatic differentiation and crustal assimilation.

5.2. Spatially and Geochemically Anomalous Arc Magmatism (SGAM) in the Andes

Our scoring system confirms that several Holocene volcanoes in the Andes are geochemically anomalous (scores of five or higher). Most of the geochemically anomalous volcanoes are also spatially anomalous (Figures 3 and 10), raising the possibility that melt generation in these localities has been driven by unique geodynamic conditions. In other words, the occurrence of SGAM may correspond to local disruptions in the normal process of melt production in subduction zones. Such disruptions can be influenced by several interlinked factors. Magmatism could be linked to the pattern of asthenospheric flow, for example, in

areas where the upwelling asthenosphere is undergoing decompression melting (Sisson & Bronto, 1998) or is responsible for transferring heat that causes partial melting in the overlying lithosphere. Related to that is the three-dimensional geometry of the subducting slab, which can influence melting. For example, the presence of slab tears can create pathways for a more complex toroidal and poloidal asthenospheric flow, with the latter promoting asthenospheric upwelling and associated melting (Faccenna & Becker, 2010; Menant et al., 2016; Rosenbaum et al., 2018). In addition, the three-dimensional geometry of slab edges influences the pattern of asthenospheric flow, which can lead to asthenospheric upwelling and associated

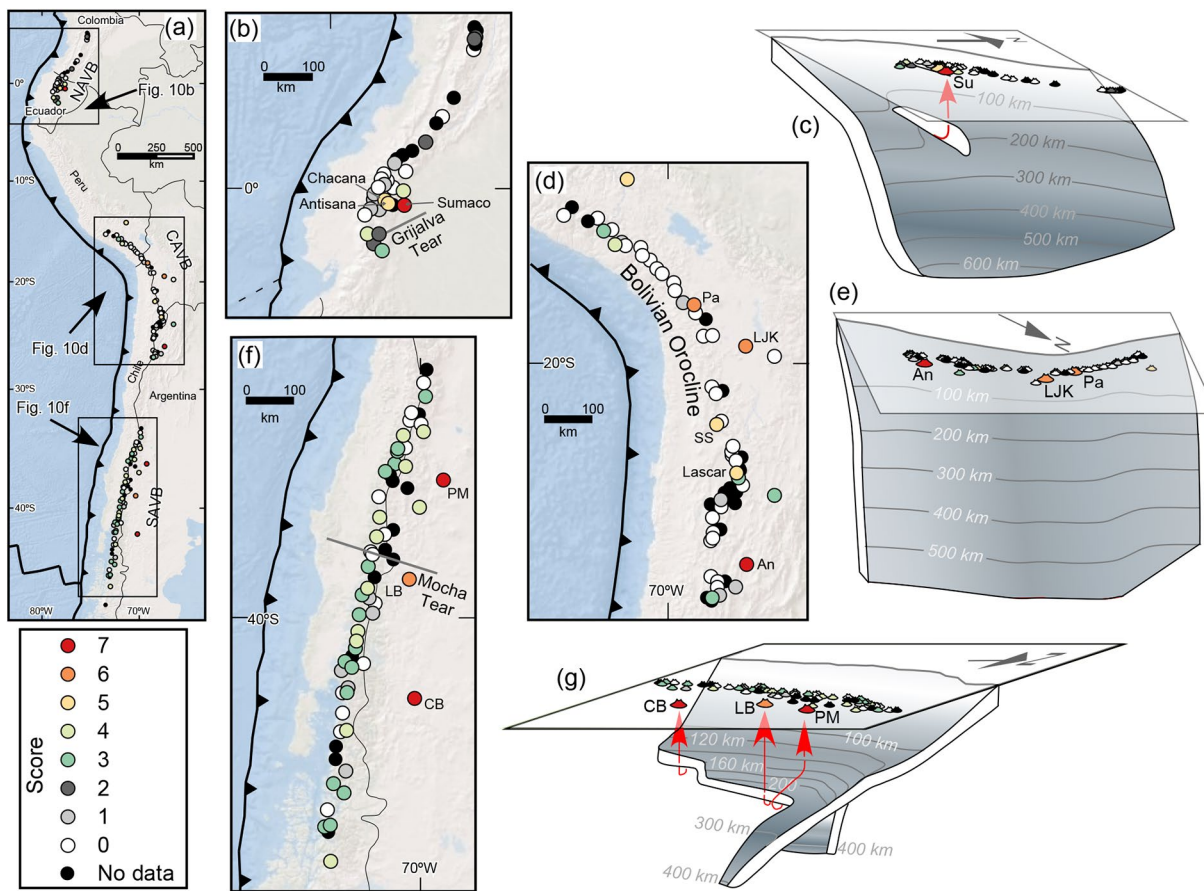


Figure 10. Maps and block diagrams highlighting locations of SGAM in the Andean belt. (a) Location map. CAVZ, Central Andean Volcanic Zone; NAVZ; Northern Andean Volcanic Zone; SAVZ, Southern Andean Volcanic Zone. (b) Northern Andes. The dashed line shows the location of the Grijalva Fracture Zone, and the thick gray line is the surface projection of the Grijalva Tear (Rosenbaum et al., 2018). (c) Schematic block diagram of the northern Andean slab and the tear underlying Sumaco. (d) Central Andes. (e) Schematic block diagram of the curved slab underlying the Bolivian Orocline. (f) Southern Andes. The thick gray line shows the surface projection of the Mocha Tear (Pesicek et al., 2012). (g) Schematic block diagram of the slab edge and Mocha Tear, underlying the Southern Andes, and their possible relationships to magmatism in Crater Basalt Volcanic Field, Laguna Blanca, and Payun Matru. Abbreviations: An, Antofagasta Volcanic Field; CB, Crater Basalt Volcanic Field; LB, Laguna Blanca; LJK, Laguna Jayu Khota; Pa, Parinacota; PM, Payun Matru; SS, San Pedro-San Pablo; Su, Sumaco.

decompression melting (Faccenna et al., 2010; Jadamec & Billen, 2010; Strak & Schellart, 2014). Lastly, the nature of melt generated, and the manner in which magmas are transferred and emplaced, are influenced by structural and compositional heterogeneities, both in the overriding plate (Acocella & Funiciello, 2010) and in the subducting plate (e.g., Chiaradia et al., 2020; Cruz-Uribe et al., 2018). Accordingly, to fully understand the spatio-geochemical distribution of arc magmatism, one must obtain detailed information on the local architecture and composition of the crust and mantle. Nevertheless, the attempt to draw a link between high geochemical anomaly scores and slab structures, as discussed below, can provide valuable insight into the origin of SGAM.

The highest geochemical anomaly scores in the Northern Andean Volcanic Zone are recorded in Sumaco (score 7), Antisana (score 5), and Chacana (score 5). These volcanoes occur in the area where the Northern Andean Volcanic Zone widens, forming a prominent cluster of volcanoes (“Ecuador cluster” in Figure 2a), including a line of seven volcanoes oriented approximately orthogonal to the slab depth contours (Quilotoa, Illiniza, Cotopaxi, Chacana, Antisana, Aliso, and Sumaco; Figure 3b). The score of these volcanoes progressively increases from west to east, with Sumaco representing the most anomalous composition (Figure 10b). The origin of Sumaco has recently been attributed to a trapdoor style tear (Grijalva Tear, Figure 10b,c) that possibly developed along the subducted segment of the Grijalva Fracture Zone to accommodate the transition from flat subduction in Peru to dipping subduction (20° – 30° ; Figure 2g) in Ecuador (Rosenbaum

et al., 2018). In this transitional zone, the slab is evidently strongly contorted, as indicated by intermediate-depth seismicity (Yepes et al., 2016), and likely torn (Rosenbaum et al., 2018). According to Rosenbaum et al. (2018), the opening of this trapdoor-style tear has exerted a poloidal mantle flow, which triggered low-degree (<3%) melting and generated the anomalous geochemical signatures observed at Sumaco. Based on the larger-scale spatial-geochemical relationships (Figure 10b, c), we suggest that the mantle dynamics associated with the Grijalva Tear is also reflected in the geochemistry of nearby volcanoes, such as Antisana and Chacana.

In the northernmost Northern Andean Volcanic Zone, evidence from intermediate-depth earthquakes and seismic tomography supports the suggestion that the slab is discontinuous and subjected to vertical tearing at latitude 5°N (Chiarabba et al., 2016; Syracuse et al., 2016; Vargas & Mann, 2013). The location of this tear coincides with the northern edge of the Northern Andean Volcanic Zone, highlighting the possibility that the disrupted slab geometry north of the tear (e.g., slab flattening, Chiarabba et al., 2016) is directly linked to the destruction of the volcanic arc. However, there is no evidence that slab tearing was accompanied by SGAM, and the paucity of geochemical data from volcanoes in central Colombia (i.e., in the northern edge of the Northern Andean Volcanic Zone; Figure 10a, b) does not allow us to assess whether melting processes were influenced by the development of the tear.

Spatially anomalous volcanoes in the northernmost Central Andean Volcanic Zone (Figure 3c), expressed by a reduced slab depth (e.g., <80 km in Sara Sara) and off-axis volcanism (Quimsachata), correspond to the transition between the Peru flat slab and the dipping slab (20–30°) underlying the Central Andean Volcanic Zone (Figure 2g). However, the recognition of geochemical anomalies in the Central Andean Volcanic Zone remains somewhat ambiguous. The vast majority (94%) of analyses from the Central Andean Volcanic Zone did not pass the SiO₂ and MgO screening tests (Figure 5), and due to the thick crust, it is difficult to recognize geochemical signatures that likely preserve diagnostic information on the original melts (e.g., see Figures 7 and 9b). We therefore emphasize that our geodynamic interpretation of high-score (≥ 5) Central Andean Volcanic Zone volcanoes remains tentative.

Two of the highest scores in the Central Andean Volcanic Zone are Antofagasta Volcanic Field (score 7) and Laguna Jayu Khota (score 6), which are both spatially anomalous, being positioned off-axis relative to the main arc and parallel to gaps in the arc front (Figures 3d, e and 10d). Furthermore, the location of Laguna Jayu Khota coincides with the area where the volcanic arc changes its orientation (Figure 3d), evidently due to the slab curvature associated with the Bolivian Orocline (Portner et al., 2020). Based on these relationships, one could speculate that slab deformation imposed by the curvature of the Bolivian Orocline (Figure 10e) is possibly linked to melt generation at Laguna Jayu Khota (e.g., in response to tears in the downdip direction of the slab). However, the idea that the slab underlying the Bolivian Orocline is torn is not supported by P-wave seismic tomography models (Chen et al., 2019; Portner et al., 2020), and suggestions of possible gaps in the slab structure (based on S-wave tomography) are not sufficiently resolved (Rodríguez et al., 2021; Scire et al., 2016). In the area underlying the Antofagasta Volcanic Field, seismic studies have identified potential magmatic bodies (Bianchi et al., 2013; Delph et al., 2017), but the origin of these have not been attributed to the geometry of the slab. Delph et al. (2017) have suggested that melt generation occurred in response to delamination of the uppermost mantle and lower crust.

The spatial context of other high scoring volcanoes in the Central Andean Volcanic Zone is less clear. Parinacota (score 6) is located at the northern limb of the Bolivian Orocline, whereas San Pedro-San Pablo and Lascar (score 5) occur in the southern limb of the orocline (Figure 10d). Quimsachata (score 5) is evidently spatially anomalous, located ~200 km from the main arc at the northernmost edge of the Central Andean Volcanic Zone. However, given that there is no evidence for slab tearing in the transition from the Central Andean Volcanic Zone to the Peru flat slab segment (Dougherty & Clayton, 2014), the geodynamic control on melt generation in Quimsachata remains an open question.

In the Southern Andean Volcanic Zone, the most anomalous compositions (score 7) belong to Crater Basalt Volcanic Field and Payun Matru (Figure 10f). Both volcanic fields occur east of the main arc, with Crater Basalt Volcanic Field located beyond the edge of the slab shown by the Slab2 model. We emphasize that, because of the limited resolution of the data used to construct the slab model, the exact location and geometry of the slab edge is ambiguous. In fact, the recent slab model by Portner et al. (2020) shows that the slab

Table 3

Summary of the Most Anomalous Volcanic Rocks (Scores 7 and 8) Found in Selected GeoROC Precompiled Files (for the Analyses, See Table S3)

GeoROC file	Location	Age	Geodynamic context
Etna Sicily	Etna, Sicily (141 analyses, score 7–8)	Quaternary	Slab tearing at the edge of a retreating slab (Gvirtzman & Nur, 1999)
Kamchatka	Central Kamchatka (10 analyses, score 7)	Quaternary	Asthenospheric window at the Kamchatka–Aleutian junction (Levin et al., 2002)
Apenninic-Maghrebides Chain	Oujda and Guilliz volcanic fields, NW Africa (10 analyses, score 7–8)	Neogene	Slab tearing at the edge of the retreating Gibraltar slab (Rosenbaum & Lister, 2004a)
Bismarck Arc – New Britain Arc	Porgera Gold Deposit, Papua New Guinea (4 analyses, score 7)	Miocene	Post-orogenic magmatism and mineralization (Holm et al., 2019)
Australia	Urannah Suite, New England Orogen (2 analyses, score 7)	Permian–Triassic	Trench retreat and backarc extension (Rosenbaum, 2018)

extends to latitude ~43°S, which is south of Crater Basalt Volcanic Field. In any case, the location of this volcanic field appears relatively close to the slab edge, thus raising the possibility that magmatism was driven by slab edge effects. Accordingly, based on the evidence of a slab melt contribution in Crater Basalt Volcanic Field (Figure 6c) and the geochemical evidence of an asthenospheric source (Massaferro et al., 2006), we suggest that this volcanic field was generated by asthenospheric flow at the slab edge (Figure 10g). Payun Matru is located in an area where the slab depth is ~220 km. The location of the other anomalous volcano, Laguna Blanca (score 6), is also off-axis relative to the main arc at a slab depth of ~180 km. Based on seismic tomography data, Pesicek et al., (2012) have suggested that a tear in the slab, at depth of >220 km, exists north of Laguna Blanca (Figure 10f). How this tear affected the pattern of mantle flow is unclear, but it is possible that it created pathways for upwelling asthenospheric material (Figure 10g). Indeed, Burd et al. (2014) have found two zones of electrically conductive structures underlying Payun Matru, which they interpreted as evidence of asthenospheric plumes. Previous authors have suggested that volcanism in Payun Matru was generated from a plume-like asthenospheric source (Germa et al., 2010; Hernando et al., 2013; Kay et al., 2004), which we think could be driven by the geometry and dynamics of the torn slab. The anomalously high values of Nb/Y in Payun Matru (Figure 9c), indicative of a slab melt contribution, support this interpretation.

5.3. Implications for Plate Tectonic Reconstructions

The recognition of SGAM highlights processes of slab tearing and segmentation, which can help reconstructing the evolution of convergent plate boundaries. Our results show that the highest geochemical anomaly scores in the northern and southern Andes are those from the spatially anomalous volcanic rocks of Sumaco, Payun Matru, and Crater Basalt Volcanic Field. These volcanic products appear to be linked to areas subjected to a complex pattern of mantle flow that formed in response to slab tearing and slab edge effects. Accordingly, the recognition of high geochemical anomaly scores in volcanic rocks from other modern and ancient arc settings may inform on similar types of processes, even in cases where the three-dimensional slab structure is no longer detectable.

To test the potential applicability of this method, we calculated geochemical anomaly scores for whole-rock analyses of volcanic rocks from convergent boundary settings, using a selection of precompiled files from the GeoROC database (Tables 3 and S3). There are caveats in this approach, such as the need to adapt thresholds when calculating geochemical anomaly scores in other arc systems, or the need to consider the influence of variable crustal thicknesses and other heterogeneities. Nevertheless, the results allow us to recognize occurrence of SGAM, showing that high geochemical anomaly scores (scores 7–8) are obtained in areas where slab tearing has been documented or postulated, such as in Mount Etna, Sicily (Gvirtzman & Nur, 1999; Schellart, 2010) and central Kamchatka (Levin et al., 2002; Portnyagin et al., 2005). In older rocks, such as Neogene rocks from the Gibraltar area (Duggen et al., 2005), the occurrence of high geochemical anomaly scores corroborates plate tectonic reconstructions that incorporated subduction segmentation, slab tearing, and the development of asthenospheric windows (Garcia-Castellanos & Villaseñor, 2011;

Rosenbaum & Lister, 2004a). Accordingly, similar types of processes might explain the origin of other subduction-related anomalous volcanic rocks, such as Permian–Triassic rocks from the New England Orogen, Australia (Allen, 2000), and Miocene mafic volcanic rocks from Porgera Gold Deposit, Papua New Guinea (Richards, 1990).

Constraining the location and timing of slab segmentation and tearing is not only important for refining tectonic reconstructions but may also provide important clues on the spatio-temporal distribution of mineral deposits. Magmas that host many porphyry deposits (as well as magmatic fluids associated with epithermal deposits) commonly deviate from the composition of typical arc-related magmas, showing, for example, enrichments in K (D. Müller & Groves, 2019). Furthermore, clusters of porphyry deposits appear to have developed at the end of magmatic cycles (Sillitoe, 1997) in areas where the subduction zone was locally disrupted, for example, due to the arrival of aseismic ridges at the subduction zone (Cooke et al., 2005; Rosenbaum et al., 2005). It is these types of processes that can lead to tearing (Hu & Liu, 2016) and associated tear-related magmatism. Metal fertility is likely inherited from the magma source (Zheng et al., 2019) and requires favorable magmatic conditions for enrichment and precipitation in the crust (e.g., Blundy et al., 2015). As such, further investigation of the coincidence of slab tearing and SGAM represents an exciting line of research into the generation of volatile- and metal-rich melts essential for ore deposit formation.

6. Conclusions

Spatio-geochemical analysis of Andean Holocene volcanoes allowed us to identify arc magmatism that is spatially and geochemically anomalous (SGAM) relative to typical arcs. We identified SGAM in the northern Andes, most evidently in Sumaco, which is situated on top of a trapdoor style slab tear that marks the transition between the Peru flat slab segment and the dipping slab underneath the Northern Andean Volcanic Zone. In the Southern Andean Volcanic Zone, the most anomalous volcanoes are identified in Payun Matru and Crater Basalt Volcanic Field, whose melting is attributed to local asthenospheric plumes associated with slab tearing and slab edge effects, respectively. Our ability to identify geochemical anomalies in the Central Andean Volcanic Zone is limited, due to the effect of magmatic fractionation within the thick crust. We note, however, that the occurrence of anomalous mafic magmatism (score 7) in Laguna Jayu Khota might be linked to slab processes associated with the curvature of the Bolivian Orocline. Our method to calculate a geochemical anomaly score for volcanic rocks provides the means to unambiguously identify anomalous magmatism in other modern and ancient convergent plate boundaries, thus offering important constraints on the role of slab tearing and segmentation in plate tectonic reconstructions.

Data Availability Statement

Datasets used in this research are presented in the Supporting Information files Table S1–S3. The original geochemical data were taken from the precompiled files “ANDEAN ARC part1.csv” and “ANDEAN ARC part2.csv” in the Georoc database (<http://georoc.mpch-mainz.gwdg.de/georoc/>). The list of Holocene volcanoes was downloaded from the Global Volcanism Program (2013) (https://volcano.si.edu/gvp_votw.cfm).

Acknowledgments

This research was funded by ARC grant DP200101566. We wish to thank Yoram Rosenbaum for help creating a database of Andean volcanoes. The manuscript benefited from comments by Agustín Cardona, three anonymous reviewers, and handling Editor Claudio Faccenna.

References

- Acocella, V., & Funiciello, F. (2010). Kinematic setting and structural control of arc volcanism. *Earth and Planetary Science Letters*, 289(1), 43–53. <https://doi.org/10.1016/j.epsl.2009.10.027>
- Allen, C. M. (2000). Evolution of a post-batholith dike swarm in central coastal Queensland, Australia: Arc-front to backarc? *Lithos*, 51(4), 331–349. [https://doi.org/10.1016/s0024-4937\(99\)00068-7](https://doi.org/10.1016/s0024-4937(99)00068-7)
- Bianchi, M., Heit, B., Jakovlev, A., Yuan, X., Kay, S. M., Sandvol, E., et al. (2013). Teleseismic tomography of the southern Puna plateau in Argentina and adjacent regions. *Tectonophysics*, 586, 65–83. <https://doi.org/10.1016/j.tecto.2012.11.016>
- Bird, P. (2003). An updated digital model of plate boundaries. *Geochemistry, Geophysics, Geosystems*, 4(3), 1027. <https://doi.org/10.1029/2001GC000252>
- Blundy, J., Mavrogenes, J., Tattitch, B., Sparks, S., & Gilmer, A. (2015). Generation of porphyry copper deposits by gas–brine reaction in volcanic arcs. *Nature Geoscience*, 8, 235–240. <https://doi.org/10.1038/ngeo2351>
- Brenan, J. M., Shaw, H. F., & Ryerson, F. J. (1995). Experimental evidence for the origin of lead enrichment in convergent-margin magmas. *Nature*, 378(6552), 54–56. <https://doi.org/10.1038/378054a0>
- Brenan, J. M., Shaw, H. F., Ryerson, F. J., & Phinney, D. L. (1995). Mineral-aqueous fluid partitioning of trace elements at 900°C and 2.0 GPa: Constraints on the trace element chemistry of mantle and deep crustal fluids. *Geochimica et Cosmochimica Acta*, 59(16), 3331–3350. [https://doi.org/10.1016/0016-7037\(95\)00215-L](https://doi.org/10.1016/0016-7037(95)00215-L)

- Burd, A. I., Booker, J. R., Mackie, R., Favetto, A., & Pomposiello, M. C. (2014). Three-dimensional electrical conductivity in the mantle beneath the Payún Matrú Volcanic Field in the Andean backarc of Argentina near 36.5°S: Evidence for decapitation of a mantle plume by resurgent upper mantle shear during slab steepening. *Geophysical Journal International*, 198(2), 812–827. <https://doi.org/10.1093/gji/ggu145>
- Caulfield, J., Turner, S., Arculus, R., Dale, C., Jenner, F., Pearce, J., et al. (2012). Mantle flow, volatiles, slab-surface temperatures and melting dynamics in the north Tonga arc-Lau back-arc basin. *Journal of Geophysical Research*, 117(B11), B11209. <https://doi.org/10.1029/2012JB009526>
- Chen, Y.-W., Wu, J., & Suppe, J. (2019). Southward propagation of Nazca subduction along the Andes. *Nature*, 565(7740), 441–447. <https://doi.org/10.1038/s41586-018-0860-1>
- Chiarabba, C., De Gori, P., Faccenna, C., Speranza, F., Seccia, D., Dionicio, V., & Prieto, G. A. (2016). Subduction system and flat slab beneath the Eastern Cordillera of Colombia. *Geochemistry, Geophysics, Geosystems*, 17(1), 16–27. <https://doi.org/10.1002/2015GC006048>
- Chiaradia, M., Müntener, O., & Beate, B. (2020). Effects of aseismic ridge subduction on the geochemistry of frontal arc magmas. *Earth and Planetary Science Letters*, 531, 115984. <https://doi.org/10.1016/j.epsl.2019.115984>
- Cooke, D., Hollings, P., & Walshe, J. L. (2005). Giant porphyry deposits—Characteristics, distribution and tectonic controls. *Economic Geology*, 100(5), 801–818. <https://doi.org/10.2113/gsecongeo.100.5.801>
- Cruz-Uribe, A. M., Marschall, H. R., Gaetani, G. A., & Le Roux, V. (2018). Generation of alkaline magmas in subduction zones by partial melting of mélange diaps—An experimental study. *Geology*, 46(4), 343–346. <https://doi.org/10.1130/G39956.1>
- Defant, M. J., & Drummond, M. S. (1990). Derivation of some modern arc magmas by melting of young subducted lithosphere. *Nature*, 347, 662–665. <https://doi.org/10.1038/347662a0>
- Delph, J. R., Ward, K. M., Zandt, G., Ducea, M. N., & Beck, S. L. (2017). Imaging a magma plumbing system from MASH zone to magma reservoir. *Earth and Planetary Science Letters*, 457, 313–324. <https://doi.org/10.1016/j.epsl.2016.10.008>
- Doglioni, C., Innocenti, F., & Mariotti, G. (2001). Why Mt Etna? *Terra Nova*, 13(1), 25–31. <https://doi.org/10.1046/j.1365-3121.2001.00301.x>
- Dougherty, S. L., & Clayton, R. W. (2014). Seismic structure in southern Peru: Evidence for a smooth contortion between flat and normal subduction of the Nazca Plate. *Geophysical Journal International*, 200(1), 534–555. <https://doi.org/10.1093/gji/ggu415>
- Drummond, M. S., & Defant, M. J. (1990). A model for trondhjemite-tonalite-dacite genesis and crustal growth via slab melting: Archean to modern comparisons. *Journal of Geophysical Research*, 95(B13), 21503–21521. <https://doi.org/10.1029/jb095ib13p21503>
- Duggen, S., Hoernle, K., Van den Bogaard, P., & Garbe-Schönberg, D. (2005). Post-collisional transition from subduction to intraplate-type magmatism in the westernmost mediterranean: Evidence for continental-edge delamination of subcontinental lithosphere. *Journal of Petrology*, 46(6), 1155–1201. <https://doi.org/10.1093/petrology/egi012>
- Errázuriz-Henao, C., Gómez-Tuena, A., Duque-Trujillo, J., & Weber, M. (2019). The role of subducted sediments in the formation of intermediate mantle-derived magmas from the Northern Colombian Andes. *Lithos*, 336–337, 151–168. <https://doi.org/10.1016/j.lithos.2019.04.007>
- Faccenna, C., & Becker, T. W. (2010). Shaping mobile belts by small-scale convection. *Nature*, 465(7298), 602–605. <https://doi.org/10.1038/nature09064>
- Faccenna, C., Becker, T. W., Lallemand, S., Lagabrielle, Y., Funiciello, F., & Piromallo, C. (2010). Subduction-triggered magmatic pulses: A new class of plumes? *Earth and Planetary Science Letters*, 299(1), 54–68. <https://doi.org/10.1016/j.epsl.2010.08.012>
- Farner, M. J., & Lee, C.-T. A. (2017). Effects of crustal thickness on magmatic differentiation in subduction zone volcanism: A global study. *Earth and Planetary Science Letters*, 470, 96–107. <https://doi.org/10.1016/j.epsl.2017.04.025>
- García-Castellanos, D., & Villaseñor, A. (2011). Messinian salinity crisis regulated by competing tectonics and erosion at the Gibraltar arc. *Nature*, 480(7377), 359–363. <https://doi.org/10.1038/nature10651>
- Garrison, J. M., Sims, K. W. W., Yogodzinski, G. M., Escobar, R. D., Scott, S., Mothes, P., et al. (2018). Shallow-level differentiation of phonolitic lavas from Sumaco Volcano, Ecuador. *Contributions to Mineralogy and Petrology*, 173, in press. <https://doi.org/10.1007/s00410-017-1431-4>
- Germa, A., Quidelleur, X., Gillot, P. Y., & Tchilinguirian, P. (2010). Volcanic evolution of the back-arc Pleistocene Payun Matrú volcanic field (Argentina). *Journal of South American Earth Sciences*, 29(3), 717–730. <https://doi.org/10.1016/j.jsames.2010.01.002>
- Gill, J. B., & Williams, R. W. (1990). Th isotope and U-series studies of subduction-related volcanic rocks. *Geochimica et Cosmochimica Acta*, 54(5), 1427–1442. [https://doi.org/10.1016/0016-7037\(90\)90166-1](https://doi.org/10.1016/0016-7037(90)90166-1)
- Global Volcanism Program. (2013). In E. Venzke (Ed.), *Volcanoes of the World*, v. 4.9.1 (17 Sep 2020). Smithsonian Institution. <https://doi.org/10.5479/lsid.GVP.VOTW4-2013>
- Grove, T. L., Chatterjee, N., Parman, S. W., & Médard, E. (2006). The influence of H₂O on mantle wedge melting. *Earth and Planetary Science Letters*, 249(1), 74–89. <https://doi.org/10.1016/j.epsl.2006.06.043>
- Gvirtzman, Z., & Nur, A. (1999). The formation of Mount Etna as the consequence of slab rollback. *Nature*, 401, 782–785. <https://doi.org/10.1038/44555>
- Hawkesworth, C., Turner, S., McDermott, F., Peate, D., & Van Calsteren, P. (1997). U-Th isotopes in arc magmas: Implications for element transfer from the subducted crust. *Science*, 276(5312), 551–555. <https://doi.org/10.1126/science.276.5312.551>
- Hayes, G. P., Moore, G. L., Portner, D. E., Hearne, M., Flamme, H., Furtnay, M., & Smoczyk, G. M. (2018). Slab2, a comprehensive subduction zone geometry model. *Science*, 362, 58–61, eaat4723. <https://doi.org/10.1126/science.aat4723>
- Hernando, I. R., Aragón, E., Frei, R., González, P. D., & Spakman, W. (2013). Constraints on the origin and evolution of magmas in the Payún Matrú Volcanic Field, Quaternary Andean back-arc of western Argentina. *Journal of Petrology*, 55(1), 209–239. <https://doi.org/10.1093/petrology/egt066>
- Hoffer, G., Eissen, J.-P., Beate, B., Bourdon, E., Fornari, M., & Cotten, J. (2008). Geochemical and petrological constraints on rear-arc magma genesis processes in Ecuador: The Puyo cones and Mera lavas volcanic formations. *Journal of Volcanology and Geothermal Research*, 176(1), 107–118. <https://doi.org/10.1016/j.jvolgeores.2008.05.023>
- Holm, R. J., Tapster, S., Jelsma, H. A., Rosenbaum, G., & Mark, D. F. (2019). Tectonic evolution and copper-gold metallogenesis of the Papua New Guinea and Solomon Islands region. *Ore Geology Reviews*, 104, 208–226. <https://doi.org/10.1016/j.oregeorev.2018.11.007>
- Hu, J., & Liu, L. (2016). Abnormal seismological and magmatic processes controlled by the tearing South American flat slabs. *Earth and Planetary Science Letters*, 450, 40–51. <https://doi.org/10.1016/j.epsl.2016.06.019>
- Hughes, G. R., & Mahood, G. A. (2008). Tectonic controls on the nature of large silicic calderas in volcanic arcs. *Geology*, 36(8), 627–630. <https://doi.org/10.1130/g24796a.1>
- Jadamec, M. A., & Billen, M. I. (2010). Reconciling surface plate motions with rapid three-dimensional mantle flow around a slab edge. *Nature*, 465, 338–341. <https://doi.org/10.1038/nature09053>

- Kay, S. M., Gorring, M. L., & Ramos, V. A. (2004). Magmatic sources, setting and causes of Eocene to recent Patagonian plateau magmatism (36°S to 52°S latitude). *Revista de la Asociación Geológica Argentina*, 59(4), 556–568.
- Kimura, J. I., Gill, J. B., Kunikiyo, T., Osaka, I., Shimoshoiri, Y., Katakuse, M., et al. (2014). Diverse magmatic effects of subducting a hot slab in SW Japan: Results from forward modeling. *Geochemistry, Geophysics, Geosystems*, 15(3), 691–739. <https://doi.org/10.1029/2013gc005132>
- Laske, G., Masters, G., Ma, Z., & Pasyanos, M. (2013). Update on CRUST1.0-A1-degree global model of Earth's crust. *Geophysical Research Abstracts*, 15
- Le Bas, M. J., Le Maitre, R. W., Streckeisen, A., & Zanettin, B. (1986). A chemical classification of volcanic rocks based on the total alkali silica diagram. *Journal of Petrology*, 27, 745–750. <https://doi.org/10.1093/petrology/27.3.745>
- Levin, V., Shapiro, N., Park, J., & Ritzwoller, M. (2002). Seismic evidence for catastrophic slab loss beneath Kamchatka. *Nature*, 418, 763–767. <https://doi.org/10.1038/nature00973>
- Mamani, M., Wörner, G., & Sempre, T. (2010). Geochemical variations in igneous rocks of the Central Andean orocline (13°S to 18°S): Tracing crustal thickening and magma generation through time and space. *GSA Bulletin*, 122(1–2), 162–182. <https://doi.org/10.1130/b26538.1>
- Mantle, G. W., & Collins, W. J. (2008). Quantifying crustal thickness variations in evolving orogens: Correlation between arc basalt composition and Moho depth. *Geology*, 36(1), 87–90. <https://doi.org/10.1130/g24095a.1>
- Massaferro, G. I., Haller, M. J., D'Orazio, M., & Alric, V. I. (2006). Sub-recent volcanism in Northern Patagonia: A tectonomagmatic approach. *Journal of Volcanology and Geothermal Research*, 155(3), 227–243. <https://doi.org/10.1016/j.jvolgeores.2006.02.002>
- McGeary, S., Nur, A., & Ben-Avraham, Z. (1985). Spatial gaps in arc volcanism: The effect of collision or subduction of oceanic plateaus. *Tectonophysics*, 119(1–4), 195–221. [https://doi.org/10.1016/0040-1951\(85\)90039-3](https://doi.org/10.1016/0040-1951(85)90039-3)
- Menant, A., Sternai, P., Jolivet, L., Guillou-Frottier, L., & Gerya, T. (2016). 3D numerical modeling of mantle flow, crustal dynamics and magma genesis associated with slab roll-back and tearing: The eastern Mediterranean case. *Earth and Planetary Science Letters*, 442, 93–107. <https://doi.org/10.1016/j.epsl.2016.03.002>
- Müller, D., & Groves, D. I. (2019). *Potassic igneous rocks and associated gold-copper mineralization* (5th ed., p. 398). Springer.
- Müller, R. D., Sdrolias, M., Gaina, C., & Roest, W. R. (2008). Age, spreading rates, and spreading asymmetry of the world's ocean crust. *Geochemistry, Geophysics, Geosystems*, 9(4), Q04006. <https://doi.org/10.1029/2007gc001743>
- Müller, R. D., Seton, M., Zahirovic, S., Williams, S. E., Matthews, K. J., Wright, N. M., et al. (2016). Ocean basin evolution and global-scale plate reorganization events since Pangea breakup. *Annual Review of Earth and Planetary Sciences*, 44(1), 107–138. <https://doi.org/10.1146/annurev-earth-060115-012211>
- Pallares, C., Maury, R. C., Bellon, H., Royer, J.-Y., Calmus, T., Aguilón-Robles, A., et al. (2007). Slab-tearing following ridge-trench collision: Evidence from Miocene volcanism in Baja California, México. *Journal of Volcanology and Geothermal Research*, 161(1), 95–117. <https://doi.org/10.1016/j.jvolgeores.2006.11.002>
- Pearce, J. A., & Peate, D. W. (1995). Tectonic implications of the composition of volcanic arc magmas. *Annual Review of Earth and Planetary Sciences*, 23(1), 251–285. <https://doi.org/10.1146/annurev.ea.23.050195.001343>
- Pesicek, J. D., Engdahl, E. R., Thurber, C. H., DeShon, H. R., & Lange, D. (2012). Mantle subducting slab structure in the region of the 2010 M8.8 Maule earthquake (30–40°S), Chile. *Geophysical Journal International*, 191(1), 317–324. <https://doi.org/10.1111/j.1365-246X.2012.05624.x>
- Plank, T., Cooper, L. B., & Manning, C. E. (2009). Emerging geothermometers for estimating slab surface temperatures. *Nature Geoscience*, 2(9), 611–615. <https://doi.org/10.1038/ngeo614>
- Plank, T., & Langmuir, C. H. (1988). An evaluation of the global variations in the major element chemistry of arc basalts. *Earth and Planetary Science Letters*, 90(4), 349–370. [https://doi.org/10.1016/0012-821x\(88\)90135-5](https://doi.org/10.1016/0012-821x(88)90135-5)
- Plank, T., & Langmuir, C. H. (1998). The chemical composition of subducting sediment and its consequences for the crust and mantle. *Chemical Geology*, 145(3), 325–394. [https://doi.org/10.1016/s0009-2541\(97\)00150-2](https://doi.org/10.1016/s0009-2541(97)00150-2)
- Portner, D. E., Rodríguez, E. E., Beck, S., Zandt, G., Scire, A., Rocha, M. P., et al. (2020). Detailed Structure of the subducted Nazca slab into the lower mantle derived from continent-scale teleseismic P Wave tomography. *Journal of Geophysical Research: Solid Earth*, 125(5), e2019JB017884. <https://doi.org/10.1029/2019jb017884>
- Portnyagin, M., Hoernle, K., Avdeiko, G., Hauff, F., Werner, R., Bindeman, I., et al. (2005). Transition from arc to oceanic magmatism at the Kamchatka-Aleutian junction. *Geology*, 33(1), 25–28. <https://doi.org/10.1130/g20853.1>
- Prelević, D., Akal, C., Romer, R. L., Mertz-Kraus, R., & Helvacı, C. (2015). Magmatic response to slab tearing: Constraints from the Afyon alkaline volcanic complex, Western Turkey. *Journal of Petrology*, 56, 527–562. <https://doi.org/10.1093/petrology/egv008>
- Profeta, L., Dueca, M. N., Chapman, J. B., Paterson, S. R., Gonzales, S. M. H., Kirsch, M., et al. (2015). Quantifying crustal thickness over time in magmatic arcs. *Scientific Reports*, 5(1), 17786. <https://doi.org/10.1038/srep17786>
- Richards, J. P. (1990). Petrology and geochemistry of alkalic intrusives at the Porgera gold deposit, Papua New Guinea. *Journal of Geochemical Exploration*, 35(1), 141–199. [https://doi.org/10.1016/0375-6742\(90\)90038-C](https://doi.org/10.1016/0375-6742(90)90038-C)
- Rodríguez, E. E., Portner, D. E., Beck, S. L., Rocha, M. P., Bianchi, M. B., Assumpção, M., et al. (2021). Mantle dynamics of the Andean subduction zone from continent-scale teleseismic S-wave tomography. *Geophysical Journal International*, 224(3), 1553–1571. <https://doi.org/10.1093/gji/gjaas36>
- Rosenbaum, G. (2018). The Tasmanides: Phanerozoic tectonic evolution of eastern Australia. *Annual Review of Earth and Planetary Sciences*, 46, 291–325. <https://doi.org/10.1146/annurev-earth-082517-010146>
- Rosenbaum, G., Gasparon, M., Lucente, F. P., Peccerillo, A., & Miller, M. S. (2008). Kinematics of slab tear faults during subduction segmentation and implications for Italian magmatism. *Tectonics*, 27, TC2008. <https://doi.org/10.1029/2007TC002143>
- Rosenbaum, G., Giles, D., Saxon, M., Betts, P. G., Weinberg, R., & Duboz, C. (2005). Subduction of the Nazca Ridge and the Inca Plateau: Insights into the formation of ore deposits in Peru. *Earth and Planetary Science Letters*, 239, 18–32. <https://doi.org/10.1016/j.epsl.2005.08.003>
- Rosenbaum, G., & Lister, G. S. (2004a). Formation of arcuate orogenic belts in the western Mediterranean region. In A. J. Sussman, & A. B. Weil (Eds.), *Orogenic curvature: Integrating paleomagnetic and structural analyses* (pp. 41–56). Geological Society of America Special Paper. [https://doi.org/10.1130/0-8137-2383-3\(2004\)383\[41:foaobt\]2.0.co;2](https://doi.org/10.1130/0-8137-2383-3(2004)383[41:foaobt]2.0.co;2)
- Rosenbaum, G., & Lister, G. S. (2004b). Neogene and Quaternary rollback evolution of the Tyrrhenian Sea, the Apennines and the Sicilian Maghrebides. *Tectonics*, 23(1), TC1013. <https://doi.org/10.1029/2003TC001518>
- Rosenbaum, G., Sandiford, M., Caulfield, J., & Garrison, J. M. (2018). A trapdoor mechanism for slab tearing and melt generation in the northern Andes. *Geology*, 47(1), 23–26. <https://doi.org/10.1130/g45429.1>

- Sandiford, D., Moresi, L. M., Sandiford, M., Farrington, R., & Yang, T. (2020). The fingerprints of flexure in slab seismicity. *Tectonics*, 39(8), e2019TC005894. <https://doi.org/10.1029/2019TC005894>
- Schellart, W. P. (2010). Mount Etna-Iblean volcanism caused by rollback-induced upper mantle upwelling around the Ionian slab edge: An alternative to the plume model. *Geology*, 38(8), 691–694. <https://doi.org/10.1130/g31037.1>
- Schiano, P., Clocchiatti, R., Ottolini, L., & Busa, T. (2001). Transition of Mount Etna lavas from a mantle-plume to an island-arc magmatic source. *Nature*, 412, 900–904. <https://doi.org/10.1038/35091056>
- Schmidt, M. W., & Poli, S. (1998). Experimentally based water budgets for dehydrating slabs and consequences for arc magma generation. *Earth and Planetary Science Letters*, 163(1), 361–379. [https://doi.org/10.1016/S0012-821X\(98\)00142-3](https://doi.org/10.1016/S0012-821X(98)00142-3)
- Scire, A., Zandt, G., Beck, S., Long, M., Wagner, L., Minaya, E., & Tavera, H. (2016). Imaging the transition from flat to normal subduction: Variations in the structure of the Nazca slab and upper mantle under southern Peru and northwestern Bolivia. *Geophysical Journal International*, 204(1), 457–479. <https://doi.org/10.1093/gji/ggv452>
- Sheldrake, T., Caricchi, L., & Scutari, M. (2020). Tectonic controls on global variations of large-magnitude explosive eruptions in volcanic arcs. *Frontiers of Earth Science*, 8(127). <https://doi.org/10.3389/feart.2020.00127>
- Sillitoe, R. H. (1974). Tectonic segmentation of the Andes: Implications for magmatism and metallogeny. *Nature*, 250(5467), 542–545. <https://doi.org/10.1038/250542a0>
- Sillitoe, R. H. (1997). Characteristics and controls of the largest porphyry copper-gold and epithermal gold deposits in the circum-Pacific region. *Australian Journal of Earth Sciences*, 44(3), 373–388. <https://doi.org/10.1080/08120099708728318>
- Sisson, T. W., & Bronto, S. (1998). Evidence for pressure-release melting beneath magmatic arcs from basalt at Galunggung, Indonesia. *Nature*, 391(6670), 883–886. <https://doi.org/10.1038/36087>
- Stern, R. J. (2002). Subduction zones. *Reviews of Geophysics*, 40(4), 3–1. <https://doi.org/10.1029/2001rg000108>
- Strak, V., & Schellart, W. P. (2014). Evolution of 3-D subduction-induced mantle flow around lateral slab edges in analogue models of free subduction analysed by stereoscopic particle image velocimetry technique. *Earth and Planetary Science Letters*, 403, 368–379. <https://doi.org/10.1016/j.epsl.2014.07.007>
- Streck, M. J., & Leeman, W. P. (2018). Petrology of “Mt. Shasta” high-magnesian andesite (HMA): A product of multi-stage crustal assembly. *American Mineralogist*, 103(2), 216–240. <https://doi.org/10.2138/am-2018-6151>
- Sun, S. S., & McDonough, W. F. (1989). Chemical and isotopic systematics of oceanic basalts: Implications for mantle composition and processes. *Geological Society, London, Special Publications*, 42(1), 313–345. <https://doi.org/10.1144/gsl.sp.1989.042.01.19>
- Syracuse, E. M., & Abers, G. A. (2006). Global compilation of variations in slab depth beneath arc volcanoes and implications. *Geochemistry, Geophysics, Geosystems*, 7(5), Q05017. <https://doi.org/10.1029/2005GC001045>
- Syracuse, E. M., Maceira, M., Prieto, G. A., Zhang, H., & Ammon, C. J. (2016). Multiple plates subducting beneath Colombia, as illuminated by seismicity and velocity from the joint inversion of seismic and gravity data. *Earth and Planetary Science Letters*, 444, 139–149. <https://doi.org/10.1016/j.epsl.2016.03.050>
- Tatsumi, Y. (2005). The subduction factory: How it operates in the evolving Earth. *Geological Society of America Today*.
- Tatsumi, Y., Hamilton, D., & Nesbitt, R. (1986). Chemical characteristics of fluid phase released from a subducted lithosphere and origin of arc magmas: Evidence from high-pressure experiments and natural rocks. *Journal of Volcanology and Geothermal Research*, 29(1–4), 293–309. [https://doi.org/10.1016/0377-0273\(86\)90049-1](https://doi.org/10.1016/0377-0273(86)90049-1)
- Till, C. B., Kent, A. J. R., Abers, G. A., Janiszewski, H. A., Gaherty, J. B., & Pitcher, B. W. (2019). The causes of spatiotemporal variations in erupted fluxes and compositions along a volcanic arc. *Nature Communications*, 10(1), 1350. <https://doi.org/10.1038/s41467-019-09113-0>
- Turner, S., Hawkesworth, C., Rogers, N., Bartlett, J., Worthington, T., Herdt, J., et al. (1997). ^{238}U - ^{230}Th disequilibrium, magma petrogenesis, and flux rates beneath the depleted Tonga-Kermadec island arc. *Geochimica et Cosmochimica Acta*, 61(22), 4855–4884. [https://doi.org/10.1016/s0016-7037\(97\)00281-0](https://doi.org/10.1016/s0016-7037(97)00281-0)
- Ubide, T., Galé, C., Larrea, P., Arranz, E., & Lago, M. (2014). Antecrysts and their effect on rock compositions: The Cretaceous lamprophyre suite in the Catalonian Coastal Ranges (NE Spain). *Lithos*, 206–207, 214–233. <https://doi.org/10.1016/j.lithos.2014.07.029>
- Vargas, C. A., & Mann, P. (2013). Tearing and breaking off of subducted slabs as the result of collision of the Panama arc-indenter with northwestern South America. *Bulletin of the Seismological Society of America*, 103(3), 2025–2046. <https://doi.org/10.1785/0120120328>
- Wilkinson, J. J. (2013). Triggers for the formation of porphyry ore deposits in magmatic arcs. *Nature Geoscience*, 6, 917–925. <https://doi.org/10.1038/ngeo1940>
- Yepes, H., Audin, L., Alvarado, A., Beauval, C., Aguilar, J., Font, Y., & Cotton, F. (2016). A new view for the geodynamics of Ecuador: Implications in seismogenic source definition and seismic hazard assessment. *Tectonics*, 35(5), 1249–1279. <https://doi.org/10.1002/2015TC003941>
- Yogodzinski, G. M., Lees, J. M., Churikova, T. G., Dorendorf, F., Wöerner, G., & Volynets, O. N. (2001). Geochemical evidence for the melting of subducting oceanic lithosphere at plate edges. *Nature*, 409, 500–504. <https://doi.org/10.1038/35054039>
- Zheng, Y.-C., Liu, S.-A., Wu, C.-D., Griffin, W. L., Li, Z.-Q., Xu, B., et al. (2019). Cu isotopes reveal initial Cu enrichment in sources of giant porphyry deposits in a collisional setting. *Geology*, 47, 135–138. <https://doi.org/10.1130/g45362.1>